Fluoride Ion Donor Properties of TcO_2F_3 and ReO_2F_3: X-ray Crystal Structures of $MO_2F_3{\cdot}SbF_5$ (M = Tc, Re) and $TcO_2F_3{\cdot}XeO_2F_2$ and Raman and NMR Spectroscopic Characterization of $MO_2F_3{\cdot}PnF_5$ (Pn = As, Sb), $[ReO_2F_2(CH_3CN)_2][SbF_6]$, and $[Re_2O_4F_5][Sb_2F_{11}]$†

Nicolas LeBlond,§ David A. Dixon,‡ and Gary J. Schrobilgen*,§

Department of Chemistry, McMaster University, Hamilton, Ontario L8S 4M1, Canada, and William R. Wiley Environmental Molecular Sciences Laboratory, Pacific Northwest National Laboratory, 906 Batelle Boulevard, P.O. Box 999, KI-83, Richland, Washington 99352

Received July 12, 1999

The fluoride ion donor properties of TcO_2F_3 and ReO_2F_3 toward AsF_5, SbF_5, and XeO_2F_2 have been investigated, leading to the formation of $TcO_2F_3{\cdot}PnF_5$ and $ReO_2F_3{\cdot}PnF_5$ (Pn = As, Sb) and $TcO_2F_3{\cdot}XeO_2F_2$, which were characterized in the solid state by Raman spectroscopy and X-ray crystallography. $TcO_2F_3{\cdot}SbF_5$ crystallizes in the monoclinic system $P2_1/n$, with a = 7.366(2) Å, b = 10.441(2) Å, c = 9.398(2) Å, β = 93.32(3)°, V = 721.6(3) Å^3, and Z = 4 at 24 °C, R_1 = 0.0649, and wR_2 = 0.1112. $ReO_2F_3{\cdot}SbF_5$ crystallizes in the monoclinic system $P2_1/c$, with a = 5.479(1) Å, b = 10.040(2) Å, c = 12.426(2) Å, β = 99.01(3)°, V = 675.1(2) Å^3, and Z = 4 at −50 °C, R_1 = 0.0533, and wR_2 = 0.1158. $TcO_2F_3{\cdot}XeO_2F_2$ crystallizes in the orthorhombic system $Cmc2_1$, with a = 7.895(2) Å, b = 16.204(3) Å, c = 5.198(1) Å, β = 90°, V = 665.0(2) Å^3, and Z = 4 at 24 °C, R_1 = 0.0402, and wR_2 = 0.0822. The structures of $TcO_2F_3{\cdot}SbF_5$ and $ReO_2F_3{\cdot}SbF_5$ consist of infinite chains of alternating MO_2F_4 and SbF_6 units in which the bridging fluorine atoms on the antimony are trans to each other. The structure of $TcO_2F_3{\cdot}XeO_2F_2$ comprises two distinct fluorine-bridged chains, one of TcO_2F_3 and the other of XeO_2F_2 bridged by long Tc−F···Xe contacts. The oxygen atoms of the group 7 metals in the three structures are cis to each other and to two terminal fluorine atoms and trans to the bridging fluorine atoms. The ^{19}F NMR and Raman spectra of $TcO_2F_3{\cdot}PnF_5$ and $ReO_2F_3{\cdot}PnF_5$ in SbF_5 and PnF_5-acidified HF solvents are consistent with dissociation of the adducts into *cis*-$MO_2F_2(HF)_2^+$ cations and PnF_6^- anions. The energy-minimized geometries of the free $MO_2F_2^+$ cations and their HF adducts, *cis*-$MO_2F_2(HF)_2^+$, have been calculated by local density functional theory (LDFT), and the calculated vibrational frequencies have been used as an aid in the assignment of the Raman spectra of the solid $MO_2F_3{\cdot}PnF_5$ adducts and their PnF_5-acidified HF solutions. In contrast, $ReO_2F_3{\cdot}SbF_5$ ionizes in SO_2ClF solvent to give the novel $Re_2O_4F_5^+$ cation and $Sb_2F_{11}^-$ anion. The ^{19}F NMR spectrum of the cation is consistent with two ReO_2F_2 units joined by a fluorine bridge in which the oxygen atoms are assumed to lie in the equatorial plane. The $[ReO_2F_2(CH_3CN)_2][SbF_6]$ salt was formed upon dissolution of $ReO_2F_3{\cdot}SbF_5$ in CH_3CN and was characterized by ^1H, ^{13}C, and ^{19}F NMR and Raman spectroscopies. The $ReO_2F_2(CH_3CN)_2^+$ cation is a pseudooctahedral *cis*-dioxo arrangement in which the CH_3CN ligands are trans to the oxygens and the fluorines are trans to each other.

Introduction

Until recently, the $ReOF_5{\cdot}SbF_5$ adduct, which is composed of the fluorine-bridged $OF_4Re{-}{-}{-}F{-}{-}{-}ReF_4O^+$ cation and the $Sb_2F_{11}^-$ anion, provided the only example of a discrete transition metal oxofluoro cation.[1] More recently, the technetium analogue $[Tc_2O_2F_9][Sb_2F_{11}]$[2] and the *cis*-dioxo $F_3O_2Os{-}{-}{-}F{-}{-}{-}OsO_2F_3^+$ cation, as the $Sb_2F_{11}^-$ salt,[3] were synthesized in this laboratory and their structures determined by X-ray crystallography. The bridging fluorines of $Re_2O_2F_9^+$, $Tc_2O_2F_9^+$, and $Os_2O_4F_7^+$ are trans to oxygens, and the oxygens of the $Os_2O_4F_7^+$ and $OsO_2F_3^+$ cations are cis to each other. The trigonal bipyramidal $OsO_2F_3^+$ cation was also observed by ^{19}F NMR spectroscopy in SbF_5 solutions of *cis*-OsO_2F_4.

Several Re^{VII} oxide fluoride cations have been observed in the mass spectrum of ReO_2F_3. The $ReO_2F_2^+$ cation was the dominant species and the $Re_2O_4F_5^+$ cation has been detected as a minor species (2%), along with $ReO_2F_3^+$ (2%) and other lower oxidation state $ReO_xF_y^+$ cations.[4]

The present work is an extension of our studies of the fluoride ion donor properties of high-valent transition metal oxide fluorides and describes the fluoride ion donor properties of TcO_2F_3 and ReO_2F_3 toward the strong fluoride ion acceptors SbF_5 and AsF_5 and the moderate fluoride ion acceptor XeO_2F_2.

Results and Discussion

The AsF_5 and SbF_5 Adducts of MO_2F_3 (M = Tc, Re). (a) Syntheses and Properties of $MO_2F_3{\cdot}SbF_5$ (M = Tc, Re). Both

† Dedicated to Professor Ronald J. Gillespie on the occasion of his 75th birthday.

§ McMaster University.

‡ Pacific Northwest National Laboratory.

(1) Schrobilgen, G. J.; Holloway, J. H.; Russell, D. R. *J. Chem. Soc., Dalton Trans.* **1984**, 1411.

(2) LeBlond, N.; Dixon, D. A.; Mercier, H. P. A.; Schrobilgen, G. J. Accepted for publication in *Inorg. Chem.*

(3) Casteel, W. J., Jr.; Dixon, D. A.; Mercier, H. P. A.; Schrobilgen, G. J. *Inorg. Chem.* **1996**, *35*, 4310.

(4) Sunder, W. A.; Stevie, F. A. *J. Fluorine Chem.* **1975**, *6*, 449.

10.1021/ic9908221 CCC: $19.00
Published on Web 05/23/2000

TcO_2F_3 and ReO_2F_3 are essentially insoluble in anhydrous HF at room temperature but dissolve readily in HF solutions acidified with the strong Lewis acids AsF_5 and SbF_5. A combining ratio of 1:1 was found when the solvent was removed from solutions containing a 3−5-fold molar excess of AsF_5 or SbF_5. The pale yellow TcO_2F_3 and colorless ReO_2F_3 adducts with SbF_5 were isolated and stored at room temperature without decomposition. In contrast, the AsF_5 adducts have significant dissociation vapor pressures of AsF_5 and revert to the starting materials when stored at room temperature.

The high solubilities of $MO_2F_3{\cdot}SbF_5$ and $MO_2F_3{\cdot}AsF_5$ in anhydrous HF apparently result from the dissociation of the adduct into $MO_2F_2^+$ cations (structure **I**) and PnF_6^- anions (eq

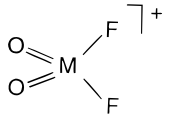

Structure I

1). The $MO_2F_2^+$ cations, however, are expected to be strong

$$MO_2F_3{\cdot}PnF_5 \overset{HF}{\rightleftharpoons} [MO_2F_2][PnF_6] \qquad (1)$$

Lewis acids and likely interact with HF. The reaction of $ReO_2F_3{\cdot}SbF_5$ with CH_3CN to form the $ReO_2F_2(CH_3CN)_2^+$ cation exemplifies the Lewis acid properties of $ReO_2F_2^+$ (eq 2).

$$ReO_2F_3{\cdot}SbF_5 \xrightarrow{CH_3CN} [ReO_2F_2(CH_3CN)_2][SbF_6] \qquad (2)$$

Attempts to prepare the $TcO_2F_2(CH_3CN)_2^+$ cation by dissolution of $TcO_2F_3{\cdot}SbF_5$ in CH_3CN at 0 °C resulted in rapid decomposition, evident from gas evolution and the formation of a dark blue solution, suggestive of the formation of a Tc^{VI} species, and was not investigated further.

The $ReO_2F_3{\cdot}SbF_5$ adduct undergoes dissociation plus self-association in SO_2ClF to form the fluorine-bridged $Re_2O_4F_5^+$ cation (structure **II**) according to eq 3. Only crystalline $ReO_2F_3{\cdot}$

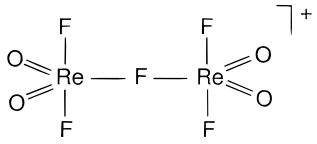

Structure II

$$2ReO_2F_3{\cdot}SbF_5 \xrightarrow{SO_2ClF} [Re_2O_4F_5][Sb_2F_{11}] \qquad (3)$$

SbF_5 could be recovered from SO_2ClF either by solvent evaporation or by crystallization from a saturated SO_2ClF solution of $ReO_2F_3{\cdot}SbF_5$ (see Experimental Section). Although $TcO_2F_3{\cdot}PnF_5$ is soluble in SO_2ClF, these solutions have not been thoroughly investigated (see Solution ^{19}F NMR Characterization of the $Re_2O_4F_5^+$ Cation).

(b) X-ray Crystal Structures of $TcO_2F_3{\cdot}SbF_5$ and $ReO_2F_3{\cdot}SbF_5$. Details of the data collection parameters and other crystallographic information are given in Table 1 and the Supporting Information. Important bond lengths, corresponding bond valences, and bond angles are listed in Table 2.

Table 1. Summary of Crystal Data and Refinement Details for $TcO_2F_3{\cdot}SbF_5$, $ReO_2F_3{\cdot}SbF_5$, and $TcO_2F_3{\cdot}XeO_2F_2$

	$TcO_2F_3{\cdot}SbF_5$	$ReO_2F_3{\cdot}SbF_5$	$TcO_2F_3{\cdot}XeO_2F_2$
space group (No.)	$P2_1/n$ (14)	$P2_1/c$ (14)	$Cmc2_1$ (36)
a (Å)	7.366(2)	5.479(1)	7.895(2)
b (Å)	10.441(2)	10.040(2)	16.204(3)
c (Å)	9.398(2)	12.426(2)	5.198(1)
β (deg)	93.32(3)	99.01(3)	90.0
V (Å^3)	721.6(3)	675.1(2)	665.0(2)
Z (molecules/unit cell)	4	4	4
mol wt	404.64	491.94	389.19
calcd density (g cm^{-3})	3.717	4.840	3.878
T (°C)	24	−50	−100
μ (mm^{-1})	8.01	11.83	9.22
final agreement factors: R_1,[a] wR_2[b]	0.0649, 0.1112	0.0533, 0.1158	0.0402, 0.0822

[a] $R_1 = \sum||F_o| - |F_c||/\sum|F_o|$. [b] $wR_2 = [\sum w(F_o^2 - F_c^2)^2/\sum w(F_o^2)^2]^{1/2}$.

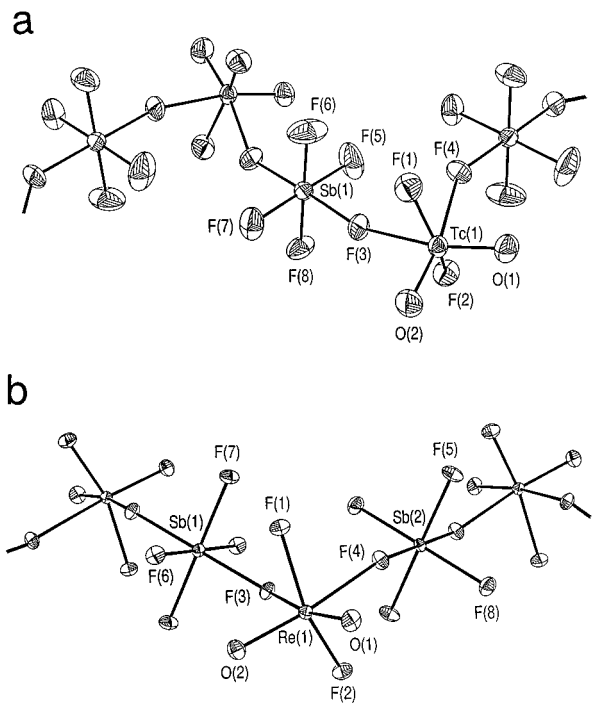

Figure 1. Structures of (a) $TcO_2F_3{\cdot}SbF_5$ and (b) $ReO_2F_3{\cdot}SbF_5$. Thermal ellipsoids are shown at the 50% probability level.

The structures of $MO_2F_3{\cdot}SbF_5$ consist of infinite chains of MO_2F_4 and SbF_6 units alternating along the b axis of the unit cell (Figure 1; and S1 (Supporting Information)). The oxygen atoms are cis to each other and trans to the bridging fluorine atoms on the transition metal but trans to each other on antimony. Both structures are closely related to that of the infinite-chain polymer $MoOF_4{\cdot}SbF_5$.[8] In both $TcO_2F_3{\cdot}SbF_5$ and $ReO_2F_3{\cdot}SbF_5$, there is one weak O···F intralayer contact (Tc complex, O(1)···F(7), 2.817 Å; and Re complex, O(2)···F(5), 2.814 Å) which is at the limit of the sum of the van der Waals radii of F and O.[9,10]

The M−O bond lengths in $MO_2F_3{\cdot}SbF_5$ are characteristic of other M^{VII}−O double bonds and are similar to the M−O bond lengths (Re values in square brackets) found in $[Li][MO_2F_4]$ (1.660(4)[11] [1.678(9)][12] Å), TcO_2F_3 (1.646(9) Å),[13] and [K]-

(5) Brown, I. D. *J. Solid State Chem.* **1974**, *11*, 214.
(6) Brown, I. D. In *Structure and Bonding in Crystals*; O'Keefe, M., Navrotsky, A., Eds.; Academic Press: London, 1981; Vol. 2, p 1.
(7) Brown, I. D.; Altermatt, D. *Acta Crystallogr.* **1985**, *B41*, 244.
(8) Fawcett, J.; Holloway, J. H.; Russell, D. R. *J. Chem. Soc., Dalton Trans.* **1981**, 1212.
(9) Pauling, L. *The Nature of the Chemical Bond*, 3rd ed.; Cornell University Press: Ithaca, NY, 1960; p 260.
(10) Bondi, A. *J. Phys. Chem.* **1964**, *68*, 441.
(11) Casteel, W. J., Jr.; Dixon, D. A.; LeBlond, N.; Mercier, H. P. A.; Schrobilgen, G. J. *Inorg. Chem.* **1998**, *37*, 340.

Table 2. Bond Lengths (Å), Bond Valences (vu), and Bond Angles (deg) in $TcO_2F_3 \cdot SbF_5$, $ReO_2F_3 \cdot SbF_5$, and $TcO_2F_3 \cdot XeO_2F_2$

$TcO_2F_3 \cdot SbF_5$

Bond Lengths and Corresponding Bond Valences[a]

Tc(1)	O(1)	O(2)	F(1)	F(2)	F(3)	F(4)
bond valence	1.965	1.949	1.084	1.073	0.351	0.347
bond length	1.640(6)	1.643(5)	1.800(5)	1.804(5)	2.217(4)	2.222(4)
total bond valence: 6.77						
Sb(1)	F(3)	F(4)	F(5)	F(6)	F(7)	F(8)
bond valence	0.704	0.702	0.895	0.898	0.890	0.871
bond length	1.927(4)	1.928(4)	1.838(5)	1.837(5)	1.840(5)	1.848(5)
total bond valence: 4.96						

Bond Angles

O(1)−Tc(1)−O(2)	103.3(3)	O(2)−Tc(1)−F(4)	169.0(3)	F(3)−Sb(1)−F(4)	179.4(2)	F(4)−Sb(1)−F(8)	89.4(2)
O(1)−Tc(1)−F(1)	101.6(3)	F(1)−Tc(1)−F(2)	146.2(2)	F(3)−Sb(1)−F(5)	91.0(2)	F(5)−Sb(1)−F(6)	89.6(4)
O(1)−Tc(1)−F(2)	99.6(3)	F(1)−Tc(1)−F(3)	76.7(2)	F(3)−Sb(1)−F(6)	89.7(3)	F(5)−Sb(1)−F(7)	179.3(2)
O(1)−Tc(1)−F(3)	166.2(2)	F(1)−Tc(1)−F(4)	77.6(2)	F(3)−Sb(1)−F(7)	89.6(2)	F(5)−Sb(1)−F(8)	90.4(3)
O(1)−Tc(1)−F(4)	87.7(2)	F(2)−Tc(1)−F(3)	76.5(2)	F(3)−Sb(1)−F(8)	90.2(2)	F(6)−Sb(1)−F(7)	90.6(3)
O(2)−Tc(1)−F(1)	100.5(3)	F(2)−Tc(1)−F(4)	77.4(2)	F(4)−Sb(1)−F(5)	89.5(2)	F(6)−Sb(1)−F(8)	179.9(3)
O(2)−Tc(1)−F(2)	99.8(3)	F(3)−Tc(1)−F(4)	78.5(2)	F(4)−Sb(1)−F(6)	90.6(2)	F(7)−Sb(1)−F(8)	89.4(3)
O(2)−Tc(1)−F(3)	90.4(2)	Tc(1A)−F(3)−Sb(1)	163.4(3)	F(4)−Sb(1)−F(7)	89.8(2)	Tc(1)−F(4)−Sb(1)	148.6(3)

$ReO_2F_3 \cdot SbF_5$

Bond Lengths and Corresponding Bond Valences[a]

Re(1)	O(1)	O(2)	F(1)	F(2)	F(3)	F(4)
bond valence	2.126	2.063	1.030	1.036	0.364	0.374
bond length	1.651(6)	1.662(6)	1.825(5)	1.823(5)	2.210(5)	2.200(5)
total bond valence: 6.99						
Sb(1)	F(3,3A)	F(6,6A)	F(7,7A)			
bond valence	0.670	0.846	0.893			
bond length	1.945(4)	1.859(5)	1.839(5)			
total bond valence: 4.82						
Sb(2)	F(4,4A)	F(5,5A)	F(8,8A)			
bond valence	0.661	0.860	0.878			
bond length	1.950(5)	1.853(5)	1.846(5)			
total bond valence: 4.80						

Bond Angles

O(1)−Re(1)−O(2)	103.2(3)	O(2)−Re(1)−F(2)	100.5(3)	F(2)−Re(1)−F(3)	78.5(2)	F(4)−Sb(2)−F(5)	89.5(2)
O(1)−Re(1)−F(1)	100.0(3)	O(2)−Re(1)−F(3)	88.5(2)	F(2)−Re(1)−F(4)	76.5(2)	F(4)−Sb(2)−F(8)	90.3(2)
O(1)−Re(1)−F(2)	99.8(3)	O(2)−Re(1)−F(4)	164.5(2)	F(3)−Re(1)−F(4)	76.0(2)	F(5)−Sb(2)−F(8)	89.0(2)
O(1)−Re(1)−F(3)	168.2(2)	F(1)−Re(1)−F(2)	147.8(2)	F(3)−Sb(1)−F(6)	89.3(2)	Re(1)−F(3)−Sb(1)	136.5(2)
O(1)−Re(1)−F(4)	92.3(2)	F(1)−Re(1)−F(3)	77.0(2)	F(3)−Sb(1)−F(7)	90.2(2)	Re(1)−F(4)−Sb(2)	149.5(3)
O(2)−Re(1)−F(1)	99.4(3)	F(1)−Re(1)−F(4)	77.6(2)	F(6)−Sb(1)−F(7)	89.9(3)		

$TcO_2F_3 \cdot XeO_2F_2$

Bond Lengths and Corresponding Bond Valences[a]

Tc(1)	O(1)	O(2)	F(1)	F(1A)	F(2,2A)
bond valence	2.120	1.992	0.491	0.541	0.970
bond length	1.612(13)	1.635(15)	2.093(13)	2.057(11)	1.840(7)
total bond valence: 7.08					
Xe(1)	O(3,3A)	F(3)	F(4)	F(2,2A)	F(4A)
bond valence	1.794	0.908	0.857	0.233	0.199
bond length	1.731(9)	1.892(13)	1.925(13)	2.848(8)	2.985(13)
total bond valence: 6.02					

Bond Angles

O(1)−Tc(1)−O(2)	101.5(8)	O(2)−Tc(1)−F(1)	169.8(7)	F(1)−Tc(1)−F(2)	79.9(3)	O(3)−Xe(1)−F(3)	91.5(4)
O(1)−Tc(1)−F(1)	88.7(6)	O(2)−Tc(1)−F(1A)	90.2(7)	F(1A)−Tc(1)−F(2)	80.1(3)	O(3)−Xe(1)−F(4)	91.1(4)
O(1)−Tc(1)−F(1A)	168.3(6)	O(2)−Tc(1)−F(2)	98.5(3)	F(2)−Tc(1)−F(2A)	153.8(5)	F(3)−Xe(1)−F(4)	175.7(6)
O(1)−Tc(1)−F(2)	98.0(3)	F(1)−Tc(1)−F(1A)	79.6(2)	O(3)−Xe(1)−O(3A)	105.6(6)		

[a] Bond valence units are defined in refs 5−7. $R_0 = 1.89$ (Tc^{VII}═O), $R_0 = 1.83$ (Tc^{VII}−F), $R_0 = 1.930$ (Re^{VII}═O), $R_0 = 1.836$ (Re^{VII}−F), $R_0 = 1.797$ (Sb^{V}−F), $R_0 = 1.971$ (Xe^{VI}═O), and $R_0 = 1.838$ (Xe^{VI}−F) were used along with $N = 3.33$ for Xe and $B = 0.37$ for Tc, Re, and Sb: Brown, I. D. Department of Physics, McMaster University, Hamilton, Ontario L8S 4M1, Canada. Private communication.

$[Re_2O_4F_7]\cdot 2ReO_2F_3$ (1.672(9), 1.680(9) Å).[12] The terminal M−F bond lengths are shorter than the lengths of the terminal M−F bonds cis to the oxygens in TcO_2F_3 (1.834(7) Å),[13] [K]-$[Re_2O_4F_7]\cdot 2ReO_2F_3$ (1.831(6), 1.854(6) Å),[12] and $[Li][MO_2F_4]$ (1.876(3)[11] [1.867(8)],[12] Å). The bridging M−F_b bonds are significantly longer than the Tc−F_b bonds in TcO_2F_3 (average 2.080(5) Å)[13] and in $[K][Re_2O_4F_7]\cdot 2ReO_2F_3$ (2.085(6), 2.119-(7) Å).[12] The decrease in the M−F and M−O bond lengths in the $MO_2F_3 \cdot SbF_5$ adducts relative to those of MO_2F_3 and $MO_2F_4^-$ and longer M−F_b bridge bonds are consistent with the increase in covalent character of the terminal M−O and M−F bonds

(12) Casteel, W. J., Jr.; Dixon, D. A.; LeBlond, N.; Lock, P. E.; Mercier, H. P. A.; Schrobilgen, G. J. *Inorg. Chem.* **1999**, *38*, 2340.
(13) Mercier, H. P. A.; Schrobilgen, G. J. *Inorg. Chem.* **1993**, *32*, 145.

expected upon partial removal of a fluoride ion from MO_2F_3 by SbF_5. The terminal Sb−F bond lengths are equal in both complexes, and despite the smaller covalent radius of technetium, the bridging M−F_b bond lengths of both MO_2F_3·SbF_5 adducts are also essentially equal. The short Re−F_b bond is indicative of the greater fluoride ion affinity, from local (LDFT) and nonlocal density functional theory (NLDFT), of ReO_2F_3 (78.0 (LDFT), 79.3 (NLDFT) kcal mol^{-1})[12] relative to that of TcO_2F_3 (74.2 (LDFT), 75.7 (NLDFT) kcal mol^{-1})[12] and is also reflected in the greater lability of the *trans*-dioxo fluorines of $TcO_2F_4^-$ [11] relative to those of $ReO_2F_4^-$ [12] in fluoride-basified anhydrous HF.

The total bond valence for the M^{VII} atom is 6.77 [6.99] vu (bond valence units), with contributions of 1.96 [2.09] vu/oxygen atom, 1.08 [1.03] vu/terminal fluorine atom, and 0.35 [0.37] vu/bridging fluorine atom. The values for the Tc−O double bonds and the Tc−F_c bonds are slightly higher than those for TcO_2F_3 (1.94 and 0.99 vu, respectively) and those for ReO_2F_3 in [K][$Re_2O_4F_7$]·2ReO_2F_3 (1.67 and 0.98 vu, respectively). The bond valence values for the M−F_b bonds of the adducts are significantly smaller than that for TcO_2F_3 (0.51 vu) and that for ReO_2F_3 in [K][$Re_2O_4F_7$]·2ReO_2F_3 (0.49 vu) and are also consistent with TcO_2F_3 and ReO_2F_3 in the roles of fluoride ion donors, with TcO_2F_3 acting as the stronger of the two donors. These findings are in accord with the relative fluoride ion affinities of TcO_2F_3 and ReO_2F_3, noted above, and with the high fluoride ion affinities of SbF_5 (120.3 kcal mol^{-1}) and AsF_5 (105.9 kcal mol^{-1}).[14]

Although the octahedra formed by the light atoms in MO_2F_3·SbF_5 are relatively undistorted (average $F_t\cdots F_b$, $F_b\cdots F_b$, $F_t\cdots O$, $F_b\cdots O$, and $O\cdots O$ distances are 2.525(7), 2.809(6), 2.647(8), 2.738(7), and 2.575(9) Å, respectively, for TcO_2F_3·SbF_5 and 2.536(7), 2.714(7), 2.667(8), 2.767(8), and 2.598(9) Å, respectively, for ReO_2F_3·SbF_5), significant distortions are observed for the coordination spheres of the metal atoms in both adducts. The VSEPR model of geometry satisfactorily accounts for these distortions,[15] with the greater spatial requirements of the oxygen double bond domains and their repulsive interactions with single bond pair domains at approximately right angles to them in the [O, F, F, F_b] planes, causing the F−M−F angle to bend away from the oxygen atoms. This angle is 146.2(2)° in TcO_2F_3·SbF_5 and 147.8(2)° in ReO_2F_3·SbF_5 and represents a significantly larger deviation from the ideal 180° angle than those found in TcO_2F_3 (154.9(3)−155.9(3)°),[13] [Li][TcO_2F_4] (164.2(3)°),[11] ReO_2F_3 in [K][$Re_2O_4F_7$]·2ReO_2F_3 (153.0(3)°),[12] and [Li][ReO_2F_4] (162.9(6)°).[12] The difference is consistent with the shorter, more covalent M−O bonds observed for MO_2F_3·SbF_5, and with their larger bond valence values, and results in stronger bond pair−bond pair repulsions than those in MO_2F_3 and [Li][MO_2F_4].

The significant variation in the M−F_b−M bridging angles within and between the two structures is noteworthy: TcO_2F_3·SbF_5 (163.4(3), 148.6(3)°); ReO_2F_3·SbF_5 (9149.5(3), 136.5(2)°). The fluorine bridge angles are intermediate with respect to those predicted for hexagonal (132°) and cubic (180°) closest packing of the fluorine atoms;[16] they were also observed to vary widely in related structures such as TcO_2F_3 (140.5(3)−153.8(3)°)[13] and [Cs][$Re_3O_6F_{10}$] (178.7(6), 140.5(4)°)[12] and are apparently strongly influenced by crystal packing.

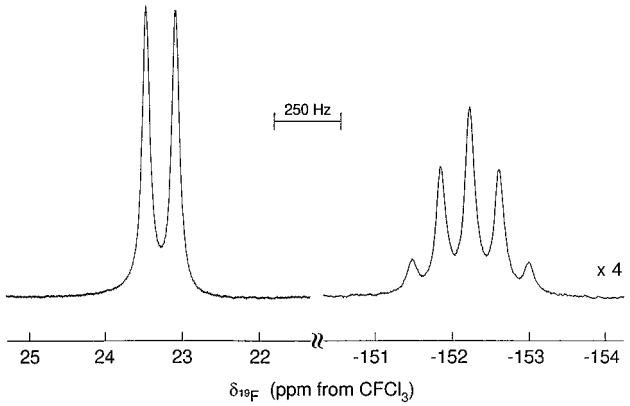

Figure 2. The ^{19}F NMR spectrum (282.409 MHz) of ReO_2F_3·SbF_5 in SO_2ClF solvent recorded at 30 °C.

(c) Solution ^{19}F NMR Characterization of the $Re_2O_4F_5^+$ Cation. The ^{19}F NMR spectrum of ReO_2F_3·SbF_5 in SO_2ClF at 30 °C (Figure 2) consists of a doublet (23.0 ppm) and a quintet (−152.8 ppm) having relative integrated intensities of 4.0:1.0, with a terminal to bridging fluorine coupling constant, $^2J(^{19}F_t-^{19}F_b)$, of 105 Hz, and is consistent with the fluorine-bridged $Re_2O_4F_5^+$ cation (structure II) (cf. $ReOF_5$: 183.4 (doublet) and −36.0 (quintet) ppm in HF; 199.0 (doublet) and −3.7 (quintet) ppm in WF_6;[17] $^2J(^{19}F_{ax}-^{19}F_{eq}) = 69$ Hz in both solvents). A broad, exchange-averaged resonance observed at −117.8 ppm ($\Delta\nu_{1/2} = 3750$ Hz) is assigned to the $Sb_2F_{11}^-$ anion. The bridging fluorine environment (quintet) is highly shielded, a feature in common with other fluorine-bridged transition metal oxofluoro species, e.g., $W_2O_2F_9^-$,[18] $Mo_2O_2F_9^-$,[19] and $Re_2O_4F_7^-$.[12] The $^2J(^{19}F_t-^{19}F_b)$ coupling constant for $Re_2O_4F_5^+$ is larger than $^2J(^{19}F_{c,c}-^{19}F_b)$ for $Re_2O_4F_7^-$ (75 Hz),[12] and comparison with $^2J(^{19}F-^{19}F)$ for OsO_2F_4 (138 Hz)[20] and $OsO_2F_3^+$ (164 Hz)[3] shows the same trend in going from a *cis*-dioxo geometry based on an octahedron to a trigonal bipyramidal arrangement where the oxygens are in the equatorial plane.

No other oxofluorides of the type $M_2O_4F_5$ have been reported, and no example of trigonal bipyramidal coordination comprising two singly fluorine-bridged MOF_3 moieties, $M_2O_2F_7$, has been characterized in solution although the structures of the $V_2O_4F_5^{3-}$ and $V_2O_2F_7^{3-}$ anions have been determined by X-ray crystallography[21] and consist of face-sharing VO_2F_4 and VOF_5 octahedra, respectively, having three bridging fluorine ligands. The $U_2O_4F_5^-$ anion has also been reported,[22] but no structural data other than an infrared spectrum, consistent with the linear geometry adopted by the UO_2 group in all other U^{VI} dioxo complexes, were reported. The $Re_2O_4F_5^+$ cation, which was only observed in SO_2ClF solution, formed the polymeric adduct ReO_2F_3·SbF_5 upon crystallization from SO_2ClF (see X-ray Crystal Structures of TcO_2F_3·SbF_5 and ReO_2F_3·SbF_5). Dissolution of TcO_2F_3·AsF_5 in SO_2ClF resulted in yellow solutions that gave rise to complex, broad ^{19}F NMR spectra at −80 °C.

(14) Christe, K. O.; Dixon, D. A.; McLemore, D.; Wilson, W. W.; Sheehy, J. A.; Boatz, J. A. *J. Fluorine Chem.* **2000**, *101*, 151.
(15) Gillespie, R. J.; Hargittai, I. *The VSEPR Model of Molecular Geometry*; Allyn and Bacon: Boston, MA, 1991.
(16) Edwards, A. J.; Jones, J. R. *J. Chem. Soc. A* **1968**, 2074.
(17) Bartlett, N.; Beaton, S.; Reeves, L. W.; Wells, E. J. *Can. J. Chem.* **1964**, *42*, 2531.
(18) Buslaev, Y. A.; Kokunov, Y. V.; Bochkareva, V. A. *J. Struct. Chem. (Engl. Transl.)* **1972**, *13*, 570; *Zh. Strukt. Khim.* **1972**, *13*, 611.
(19) Buslaev, Y. A.; Kokunov, Y. V.; Bochkareva, V. A.; Shostorovich, E. M. *J. Struct. Chem. (Engl. Transl.)* **1972**, *13*, 491; *Zh. Strukt. Khim.* **1972**, *13*, 526.
(20) Christe, K. O.; Dixon, D. A.; Mack, H. G.; Oberhammer, H.; Pagelot, A.; Sanders, J. C. P.; Schrobilgen, G. J. *J. Am. Chem. Soc.* **1993**, *115*, 11279.
(21) Buchholz, N.; Leimkühler, M.; Kiriazis, L.; Mattes, R. *Inorg. Chem.* **1988**, *27*, 2035.
(22) Davidovich, R. L.; Zemskova, L. A. *Russ. Chem. Bull. (Engl. Transl.)* **1978**, 1492; *Izv. Akad. Nauk SSSR, Ser. Khim.* **1978**, 1708.

(d) Solution ^{19}F and ^{99}Tc NMR Studies of the Reactions of MO_2F_3 with AsF_5 and SbF_5. The ^{19}F NMR spectrum of $TcO_2F_3 \cdot AsF_5/5AsF_5$ in HF at −84 °C consists of a broad singlet at 109.2 ppm ($\Delta\nu_{1/2} = 438$ Hz), which is significantly deshielded compared to the fluorine resonances of $TcO_2F_3(CH_3CN)$ (25.3 and 37.3 ppm in CH_3CN at 30 °C) and $TcO_2F_4^-$ (−14.1 and −18.7 ppm in CH_3CN; 23.0 ppm in HF) and is consistent with the formation of the $TcO_2F_2^+$ cation. Broad resonances at −67.9 ($\Delta\nu_{1/2} = 3500$ Hz) and −124.9 ppm ($\Delta\nu_{1/2} = 2500$ Hz) are assigned to AsF_6^- and exchange-averaged AsF_5 and HF, respectively. The ^{19}F NMR spectrum, recorded at 30 °C, consists of a singlet at −134.7 ppm ($\Delta\nu_{1/2} = 1675$ Hz) and is the result of rapid fluorine exchange among HF, AsF_5, AsF_6^-, and fluorine on Tc^{VII}. The ^{99}Tc NMR spectrum of $TcO_2F_3 \cdot AsF_5/5AsF_5$ in HF at −54 °C is a singlet at 140.3 ppm ($\Delta\nu_{1/2} = 2500$ Hz) which is broadened by fast quadrupolar relaxation of the ^{99}Tc nucleus ($I = {}^9/_2$; $Q = -0.129(6) \times 10^{-28}$ m^2).[11] Sharpening of the ^{99}Tc NMR signal occurs at 30 °C (143.2 ppm; $\Delta\nu_{1/2} = 793$ Hz) but is not sufficient to observe the $^1J(^{99}Tc-^{19}F)$ coupling. The ^{99}Tc resonance is deshielded relative to that of TcO_3F in HF (43.7 ppm)[23] but is similar to that of TcO_3^+ in HF (160.7 ppm).[23] The ^{19}F NMR spectrum of $TcO_2F_3 \cdot SbF_5$ in HF recorded at −80 °C comprises two broad resonances at 106.8 ($\Delta\nu_{1/2} =$ 1000 Hz) and −127.8 ppm ($\Delta\nu_{1/2} = 2350$ Hz) and an intense, sharp singlet at −193.7 ppm ($\Delta\nu_{1/2} = 30$ Hz), which are assigned to fluorine on Tc^{VII}, SbF_6^-, and HF solvent, respectively. An attempt was made to slow the fluorine exchange by dissolving TcO_2F_3 in neat SbF_5, but the high viscosity of SbF_5 increased the quadrupolar relaxation rate of ^{99}Tc, resulting in a very broad ^{99}Tc resonance, even at 64 °C (128.4 ppm; $\Delta\nu_{1/2} =$ 18 600 Hz). The ^{19}F NMR spectrum of this solution recorded at 30 °C yielded a broad resonance at −114.1 ppm ($\Delta\nu_{1/2} =$ 4700 Hz) assigned to SbF_5 exchange-averaged with $Sb_nF_{5n+1}^-$ and a singlet at 137.5 ppm ($\Delta\nu_{1/2} = 106$ Hz) which is in good agreement with the F-on-Tc^{VII} resonance obtained for $TcO_2F_3 \cdot MF_5$ dissolved in HF acidified with MF_5.

The ^{19}F NMR spectra of HF solutions of $ReO_2F_3 \cdot AsF_5/5AsF_5$ and $ReO_2F_3 \cdot SbF_5/5SbF_5$ at 30 °C each display a singlet in the fluorine-on-rhenium(VII) region of the spectrum. These resonances are broadened because of fluorine exchange with the solvent and occur at 19.8 ($\Delta\nu_{1/2} = 1625$ Hz) and 24.4 ppm ($\Delta\nu_{1/2} = 1550$ Hz) for HF solutions of $ReO_2F_3 \cdot AsF_5$ and $ReO_2F_3 \cdot SbF_5$, respectively. The spectrum of $ReO_2F_3 \cdot AsF_5/5AsF_5$ also displays an intense singlet at −163.5 ppm ($\Delta\nu_{1/2} =$ 210 Hz) assigned to HF, AsF_5, and AsF_6^- undergoing rapid fluorine exchange. The spectrum of $ReO_2F_3 \cdot SbF_5/5SbF_5$ displays two additional resonances at −125.3 ppm ($\Delta\nu_{1/2} = 2380$ Hz) in the F-on-Sb^V region of the spectrum assigned to SbF_5 exchange-averaged with SbF_6^- and a resonance at −193.0 ppm ($\Delta\nu_{1/2} = 400$ Hz) assigned to HF. The low-temperature (−80 to −90 °C) ^{19}F NMR spectra of $ReO_2F_3 \cdot PnF_5$ in HF and in PnF_5-acidified HF solutions are complex and are not treated in the present work, but they suggest equilibria involving the formation of fluorine-bridged oligomeric cations. Dissolution of ReO_2F_3 in neat SbF_5 slowed intermolecular fluorine exchange sufficiently at 30 °C to give a singlet at 37.4 ppm ($\Delta\nu_{1/2} = 200$ Hz) in the F-on-Re^{VII} region of the spectrum. Intense, broad ^{19}F resonances arising from polymeric $(SbF_5)_n/Sb_nF_{5n+1}^-$ were also observed at −86.2 ($\Delta\nu_{1/2} = 1500$ Hz), −104.7 ($\Delta\nu_{1/2} =$ 1100 Hz), and −132.0 ppm ($\Delta\nu_{1/2} = 1350$ Hz). The chemical shifts corresponding to fluorine on Re^{VII} observed in HF solutions of $ReO_2F_3 \cdot PnF_5$ acidified with PnF_5 and of ReO_2F_3 in neat SbF_5 are very similar to the chemical shift of the four equivalent terminal fluorines of the $Re_2O_4F_5^+$ cation (23.0 ppm, doublet; vide supra).

The ^{19}F and ^{99}Tc chemical shift behaviors of MO_2F_3 in strong fluoride ion acceptor media are consistent with the formation of $MO_2F_2^+$ cations that are likely to interact with the solvent media, HF and SbF_5, by formation of fluorine bridges, such as in the HF solvate *cis*-$MO_2F_2(FH)_2^+$ (vide infra).

(e) Raman Spectra of $MO_2F_3 \cdot PnF_5$. The Raman spectra of $TcO_2F_3 \cdot PnF_5$ and $ReO_2F_3 \cdot PnF_5$ (Pn = As, Sb) as solids and in HF solution are shown in Figures 3 and 4 and frequencies and their assignments are listed in Tables 3 and 4, respectively. Frequencies have also been calculated at several levels of theory for the tetrahedral $MO_2F_2^+$ cations in the gas phase and for the *cis*-dioxo $MO_2F_2^+$ cations fluorine-bridged to two HF molecules and have mainly been used to assign the spectra (see Theoretical Calculations). Assignments were also confirmed by comparison with those for polymeric TcO_2F_3[13] and ReO_2F_3,[12] $TcO_2F_4^-$,[11] and $ReO_2F_4^-$.[12] Spectral assignments for $MO_2F_3 \cdot PnF_5$ in HF solution were also aided by polarization measurements. The assignments of the fluorine-bridged PnF_6 groups in the solid state and of PnF_6^- in HF solution were made by comparison with their oxonium and alkali metal salts.[24,25]

In accord with the crystal structures of $TcO_2F_3 \cdot SbF_5$ and $ReO_2F_3 \cdot SbF_5$, the spectra of the solid adducts were interpreted in terms of the local symmetries of the *cis*-MO_2F_4 units (C_{2v} point symmetry) and the PnF_6 units (D_{4h} point symmetry). The approach is approximate and does take into account vibrational coupling within the polymer chain, including the coupled M---F---Pn bridging stretching and bending modes. Partially resolved vibrational band splittings, consistent with the couplings that are observed on several bands, are not explicitly assigned but are assigned under the local symmetries of the MO_2F_4 and PnF_6 units.

Although the assignments in HF solution are given for the "$MO_2F_2^+$ cation", strong interactions between the cations and the solvent are likely to occur because of the expected strong Lewis acid characters of the $MO_2F_2^+$ cations. The simplicity of the solution spectra and their similarity to those of the solid adducts suggest that the $MO_2F_2^+$ cations are the dominant species and are coordinated to two HF solvent molecules, resulting in a *cis*-$MO_2F_2F_{2b}$ moiety (where F_b is the bridging fluorine of coordinated HF) having C_{2v} point symmetry. Consequently, the vibrational modes of "$MO_2F_2^+$" are assigned under the assumed C_{2v} point symmetry for HF-solvated *cis*-dioxo $MO_2F_2(FH)_2^+$ cations.

The intense MO_2 and terminal metal−fluorine stretching modes are shifted to significantly higher frequencies both in the solid state and in solution when compared to those of MO_2F_3,[12,13] consistent with partial removal of fluoride ion. The antisymmetric and symmetric bridging MF_{2b} stretching modes of the solid adducts are assigned to the bands at 576 and 552 [570 and 517] cm^{-1} and 492 and 541 [542 and 503] cm^{-1}, respectively, on the basis of their broad, weak peak profiles, which are typical features in the spectra of other fluorine-bridged species.[3] The MO_2 scissoring modes at 413, 416, and 410 [411 and 407] cm^{-1} in the solid adducts and at 409 and 407 [404 and 403] cm^{-1} in HF solution are consistent features in the Raman spectra of *cis*-dioxo transition metal complexes and are in close agreement with those of TcO_2F_3 (411 cm^{-1})[13] and ReO_2F_3 (412 cm^{-1}).[12] The assignments of the remaining

(23) Franklin, K. J.; Lock, C. J. L.; Sayer, B. G.; Schrobilgen, G. J. *J. Am. Chem. Soc.* **1982**, *104*, 5303.
(24) Begun, G. M.; Rutenberg, A. C. *Inorg. Chem.* **1967**, *6*, 2212.
(25) Christe, K. O.; Charpin, P.; Soulie, E.; Bougon, R.; Fawcett, J.; Russell, D. R. *Inorg. Chem.* **1984**, *23*, 3756.

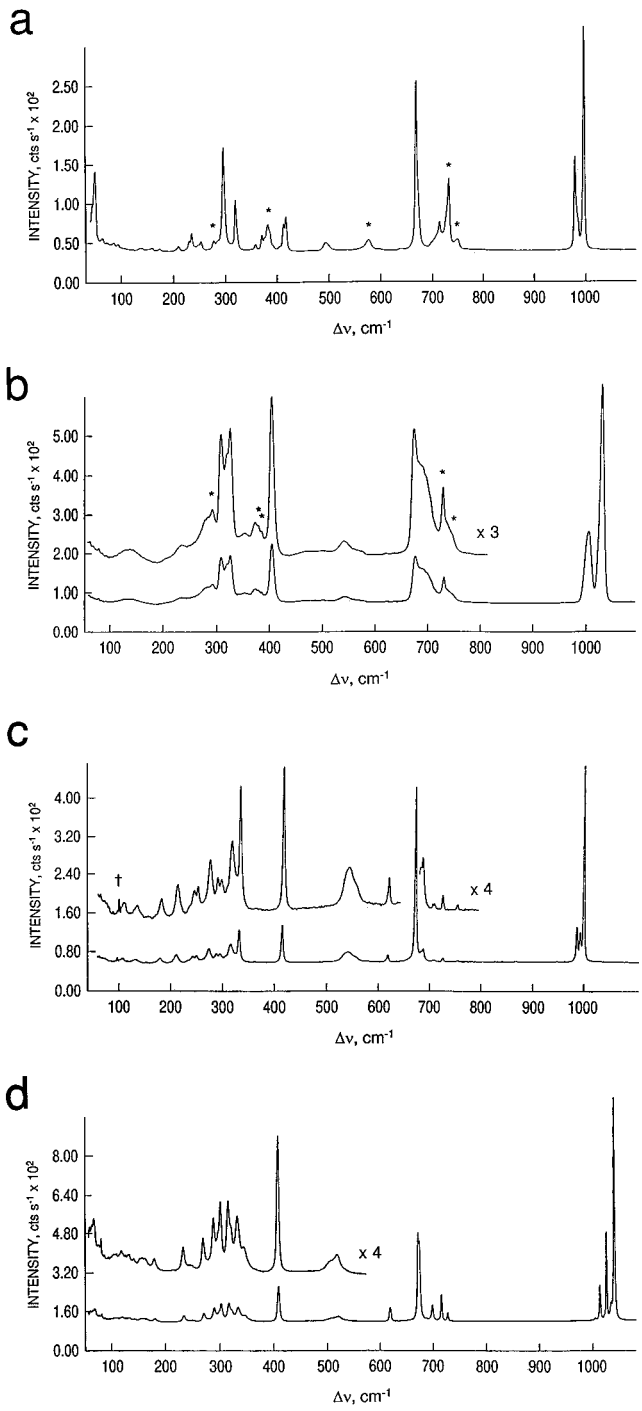

Figure 3. Raman spectra of microcrystalline (a) $TcO_2F_3 \cdot AsF_5$ and (b) $ReO_2F_3 \cdot AsF_5$ recorded in FEP at −150 °C using 514.5-nm excitation and (c) $TcO_2F_3 \cdot SbF_5$ (647.1-nm excitation) and (d) $ReO_2F_3 \cdot SbF_5$ (514.5-nm excitation) recorded in Pyrex melting point capillaries at 23 °C. The dagger (†) denotes a plasma line, and asterisks (*) denote FEP sample tube lines.

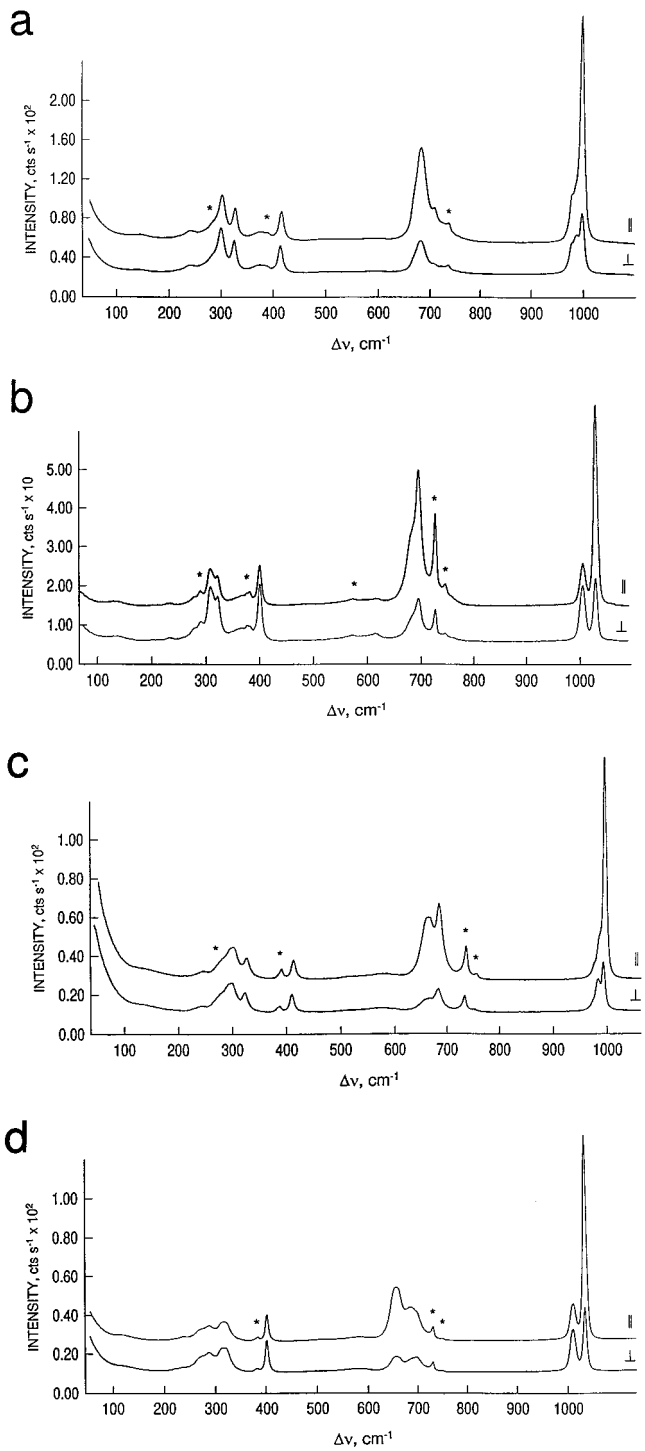

Figure 4. Raman spectra of HF solutions of (a) $TcO_2F_3 \cdot AsF_5$, (b) $ReO_2F_3 \cdot AsF_5$, (c) $TcO_2F_3 \cdot SbF_5$, and (d) $ReO_2F_3 \cdot SbF_5$ recorded in FEP at 23 °C using 514.5-nm excitation, with the analyzer oriented parallel (∥) and perpendicular (⊥) to the polarization of the incident beam. Asterisks (*) denote FEP sample tube lines.

deformation modes are more tentative. The symmetric terminal fluorine stretching modes for the AsF_6 and SbF_6 units under D_{4h} symmetry in the solid adducts are assigned to the high-intensity bands at 669 [677] and 668, 678, 682 [670, 672] cm^{-1}, respectively. The corresponding out of phase modes for the AsF_6 and SbF_6 units are assigned at lower frequencies to bands at 640 and 613 [616] cm^{-1}, respectively. The in-plane bending modes of the terminal fluorines in the AsF_6 and SbF_6 units are assigned at 370 [372] and 286 [286] cm^{-1}, respectively, and are in good agreement with their counterparts in the spectra of octahedral PnF_6^- anions.[24,25] Because PnF_5 and hence $Pn_nF_{5n+1}^-$ ($n = 1$ or 2) are present in large excess in HF solutions of the adducts, the relative intensities of the $Pn_nF_{5+1}^-$ modes in these solutions are more intense than would be expected for the stoichiometric compound.

(f) Theoretical Calculations. The calculated structures and vibrational frequencies at the local density functional theory

Table 3. Raman Frequencies, Assignments and Mode Descriptions for Solid TcO_2F_3·PnF_5 and ReO_2F_3·PnF_5 (Pn = As, Sb)

freq[a] (cm^{-1})				assignt[b]	
TcO_2F_3·AsF_5[c]	TcO_2F_3·SbF_5[d]	ReO_2F_3·AsF_5[c]	ReO_2F_3·SbF_5[d]	$F_{2b}MO_2F_2$ (C_{2v})	F_4PnF_{2b} (D_{4h})
997 (100)	995 (100)	1035 (100)	1040 (100)	A_1, $\nu_s(MO_2)$	
985, sh 979 (23), sh	982 (14) 972 (17)	1009 (32)	1025 (39) 1013 (16)	B_1, $\nu_{as}(MO_2)$	
e	746 (<1)	~740[e]		B_2, $\nu_{as}(MF_2)$[e]	
727, sh[e] 714 (15)	721 (2)	727 (10)	724 (4) 713 (11)	A_1, $\nu_s(MF_2)$	
700, sh	702 (<1) 699 (<1)[f]		696 (6)		E_u, $\nu_{as}(SbF_4)$
		694, sh			E_u, $\nu_{as}(AsF_4)$
	682 (6) 678 (5), sh 668 (89)		672 (6) 670 (39)		A_{1g}, $\nu_s(SbF_4)$
669 (80)		677 (20)			A_{1g}, $\nu_s(AsF_4)$
640 (<1), sh					B_{1g}, $\nu_s(AsF_4)$, o.p.
	613 (3)		616 (6)		B_{1g}, $\nu_s(SbF_4)$, o.p.
576 (5) 492 (4)	552 (2), sh 541 (5)	570 (1), br 542 (2), br	517 (2), br 503 (1), br		A_{2u}, $\nu_{as}(PnF_{2b})$;[g] A_{1g}, $\nu_s(PnF_{2b})$[g]
416 (21) 413 (12), sh	410 (19)	404 (27)	407 (15)	A_1, $\delta_{sc}(MO_2)$	
370 (7)		372 (6)			B_{2g}, $\delta_{sc}(AsF_4)$
357 (2)		351 (4)			E_g, $\delta(AsF_2F_{2b})$
			342 (2)	*h*	
319 (25)	328 (16)	325 (21) 318 (17), sh	330 (6) 318 (6), sh	B_2, $\rho_w(MO_2)$	
	312 (9) 301 (3), sh	307 (20)	313 (8) 298 (8)	A_1, $\nu_s(MF_{2b})$;B_1, $\nu_{as}(MF_{2b})$	
295 (51)	291 (4)	291 (8)	294 (6), sh	A_2, $\delta(OMF)/\rho_t(MO_2)$	
	286 (4)		286 (6)		B_{2g}, $\delta_{sc}(SbF_4)$
276 (4)		277 (6), sh		*h*	
	270 (6)		266 (4)		E_g, $\delta(SbF_2F_{2b})$
252 (4) 246 (3), sh	248 (3) 241 (3)	240 (2) 232 (3)	245 (<1) 229 (3)	B_1, $\rho_w(MF_2)$	
234 (9) 230 (5), sh	230 (1), sh	201 (1)		A_1, $\delta_{sc}(MF_2)$	
208 (3)	207 (4)			A_1, $\delta_{sc}(MF_{2b})$	
171 (1)	178 (3)		176 (1)	B_2, $\rho_w(MF_{2b})$	
157 (1)			158 (1) 151 (1)	B_1, $\rho_t(MO_2)$	
136 (1) 120 (<1)	127 (2)	132 (3), br	137 (<1) 129 (1) 126 (<1)	δ(Pn-F---M)	
			114 (1)	lattice modes	
104 (<1) 92 (2) 48 (42)	105 (2)		105 (<1) 98 (<1) 89 (2)		
83 (2)			81 (4)	A_2, $\rho_t(MF_{2b})$	

[a] Values in parentheses denote relative Raman intensities. Abbreviations denote shoulder (sh) and broad (br). [b] The 15 vibrational modes of the $MO_2F_2F_{2b}$ units belong to the irreducible representations $6A_1 + 2A_2 + 4B_1 + 3B_2$ (the [O, O, M, F_b, F_b] plane is taken as the $\sigma_v(xz)$ plane with the *z* axis as the C_2 axis), and all are Raman and infrared active except the A_2 modes, which are only Raman active. The vibrational modes for the PnF_6 units belong to the irreducible representations $2A_{1g} + B_{1g} + B_{2g} + E_g + 2A_{2u} + B_{2u} + 3E_u$, of which the A_{1g}, B_{1g}, B_{2g}, and E_g modes are Raman active and the A_{2u} and E_u modes are infrared active. Symbols denote stretching (ν), bend (δ), scissors bend (δ_{sc}) in the MO_2 or MF_{2b} plane, wag (ρ_w), rock (ρ_r), and torsion (ρ_t). F denotes a terminal fluorine cis to oxygens and F_b a bridging fluorine in an M---F_b---Pn bridge; o.p. denotes out of phase. [c] Spectrum recorded on the microcrystalline solid in FEP at −150 °C using 514.5-nm excitation. [d] Spectrum recorded on the microcrystalline solid in a rotating Pyrex glass capillary at 23 °C using 647.1-nm (Tc) and 514.5-nm (Re) excitations. [e] The bands corresponding to $\nu_{as}(MF_2)$ are expected to be weak and, in the cases of TcO_2F_3·AsF_5 and TcO_2F_3·SbF_5, may coincide with FEP sample tube lines at 734 (100) and 752 (9) cm^{-1}. [f] These bands may be assigned to formally inactive Raman stretches (E_u and A_{2u}) which are visible because of factor group splitting within the unit cell. [g] These bands cannot be unambiguously assigned to either A_{2u}, $\nu_{as}(PnF_{2b})$ or A_{1g}, $\nu_s(PnF_{2b})$. The formal Raman inactivity of the A_{2u} mode suggests that it should be the weaker line. [h] Unassigned band.

Table 4. Raman Frequencies, Assignments, and Mode Descriptions for $TcO_2F_3 \cdot PnF_5$ and $ReO_2F_3 \cdot PnF_5$ (Pn = As, Sb) in HF Solution[a]

freq[b] (cm^{-1})				assignt[c]
$TcO_2F_3 \cdot AsF_5$	$TcO_2F_3 \cdot SbF_5$	$ReO_2F_3 \cdot AsF_5$	$ReO_2F_3 \cdot SbF_5$	MO_2F_2 (C_{2v})
992 (100), p	993 (100), p	1037 (100), p	1035 (100), p	A_1, $\nu_s(MO_2)$
972 (23), sh, dp	981 (18), sh, dp	1012 (22), dp	1011 (20), dp	B_1, $\nu_{as}(MO_2)$
d	*d*	740[d]	*d*	B_2, $\nu_{as}(MF_2)$
701 (15)	680 (34), p	701 (54), p	689 (16), p	A_1, $\nu_s(MF_2)$
676 (42), p	655 (30), p	687 (31), sh, p	658 (26), p	*e*
664, sh, dp	662, sh, dp	620 (2), dp		*e*
	507 (<1), dp		503 (<1), dp	*e*
409 (15), dp	407 (10), dp	404 (18), dp	403 (20), dp	A_1, $\delta_{sc}(MO_2)$
375 (6), dp		371 (5), sh, dp		*e*
321 (17), dp	321 (1), dp	325 (13), dp	321 (12), dp	B_2, $\rho_w(MO_2)$
		311 (16), dp		A_1, $\nu_s(MF_{2b})$; B_1, $\nu_{as}(MF_{2b})$
295 (24), dp	296 (15), dp	293 (6), dp	289 (8), dp	A_2, $\delta(OMF)/\rho_t(MO_2)$
	290 (15), sh, dp	280 (3), dp	277 (7), sh, dp	*e*
	274 (10), sh, dp			*e*
234 (6), dp	239 (4), dp	236 (1), dp	239 (3), dp	B_1, $\rho_w(MF_2)$
			223 (2), dp	A_1, $\delta_{sc}(MF_2)$
132 (4), dp		134 (2), dp	122 (2), dp	*e*

[a] Spectra were recorded in FEP sample tubes at 23 °C using 514.5 nm excitation. [b] See Table 3, footnote *a*; other abbreviations denote polarized (p) and depolarized (dp). [c] The $MO_2F_2F_{2b}$ units of the solvated cations, *cis*-dioxo $MO_2F_2(F_bH)_2$, are assigned by analogy with those of the solid $MO_2F_3 \cdot PnF_5$ adducts (see Table 3, footnote *b*). F denotes a terminal fluorine cis to oxygens, and F_b is a bridging fluorine in an M---F_b—H bridge; remaining symbols are defined in Table 3, footnote *b*. [d] Weak line likely obscured by overlap with FEP sample tube lines at 734 (100) and 752 (9) cm^{-1}. [e] Assigned to $Pn_5F_{5n+1}^-$, where $n = 1$ and 2 likely dominate.

Table 5. Predicted LDFT Geometries for $MO_2F_2^+$ and MO_4^- (M = Tc, Re)[a]

		free $TcO_2F_2^+$				TcO_4^-			
geometric parameter	expt for solid adduct[b]	all-electron[c]	HW[d]	EC[e]	free *cis*-$TcO_2F_2(FH)_2^+$ all-electron[c]	exp.[f]	all-electron[c]	HW[d]	EC[e]
Tc—O	1.642	1.668	1.662	1.661	1.676	1.711(3), 1.724[g]	1.742	1.738	1.735
Tc—F	1.802	1.801	1.795	1.793	1.823				
∠OTcO	103.3	105.9	105.6	105.6	104.3	110.5(2), 109.0(2)	109.5	109.5	109.5
∠FTcF	146.2	113.5	116.1	116.1	137.9				
∠FTcO	100.4	109.3	109.2	108.6	102.7				
Tc---F_b(H)	2.220				2.318				

		free $ReO_2F_2^+$				ReO_4^-			
geometric parameter	expt for solid adduct[h]	PP[i]	HW[d]	EC[e]	free *cis*-$ReO_2F_2(FH)_2^+$ EC[e]	expt.[f]	PP[i]	HW[d]	EC[e]
Re—O	1.656	1.684	1.670	1.668	1.673	1.719(5), 1.733[g]	1.755	1.740	1.740
Re—F	1.811	1.811	1.798	1.795	1.817				
∠OReO	103.2	105.5	105.0	105.0	103.6	110.2, 109.2	109.5	109.5	109.5
∠FReF	147.8	116.7	117.8	117.8	138.5				
∠FReO	99.9	108.5	108.3	108.3	102.6				
Re---F_b(H)	2.205				2.343				

[a] Bond distances in angstroms and bond angles in degrees. [b] Average values for $TcO_2F_3 \cdot SbF_5$ taken from Table 2. [c] All-electron calculation with a DZVP basis set. [d] Hay—Wadt ECP (refs 26—28) + DZVP2 basis set. [e] Ermler-Christiansen ECP's (refs 29, 30) + DZVP2 basis set. [f] Reference 31. [g] Value corrected for librational oscillations. [h] Average values for $ReO_2F_3 \cdot SbF_5$ taken from Table 2. [i] PP (refs 32, 33) + DZVP2.

(LDFT) level are given in Tables 5 and 6,[26—34] respectively, for $TcO_2F_2^+$ and $ReO_2F_2^+$ and for their adducts with two HF molecules. We also report the calculated geometries (Table 5) and vibrational frequencies (Table 6) for TcO_4^- and ReO_4^-, which show good overall agreement between the different methods for TcO_4^-, with the all-electron and ECP results being quite similar. For ReO_4^-, the PP results differ from the ECP results by more than might be expected, especially for the frequencies of the bending modes. For $TcO_2F_2^+$, there are only small differences between the all-electron calculations and those done with the ECPs. We did not perform PP calculations for Tc because, in our prior experience, we did not obtain good geometries. The geometries around the metals are pseudotetrahedral, with the O—M—O angle smaller than the ideal angle of 109.5° and the F—M—F angle opened up from the ideal angle, and are opposite to trends based on VSEPR considerations. The difference is accounted for by a π interaction (NHOMO) and a σ interaction (HOMO-3) between the cis oxygens. Addition of two HF molecules to mimic the fluorine bridge interactions in the adducts and solvation of the $MO_2F_2^+$ cations in HF solvent had a significant impact on the cation geometries. The HF molecules are weakly complexed to the cation with (H)F_b---M

(26) Hay, P. J.; Wadt, W. R. *J. Chem. Phys.* **1985**, *82*, 270.
(27) Hay, P. J.; Wadt, W. R. *J. Chem. Phys.* **1985**, *82*, 284.
(28) Hay, P. J.; Wadt, W. R. *J. Chem. Phys.* **1985**, *82*, 299.
(29) Ermler, W. C.; Ross, R. B.; Christiansen, P. A. *Adv. Quantum Chem.* **1988**, *19*, 139.
(30) Ross, R. B.; Powers, J. M.; Atashroo, T.; Ermler, W. C.; LaJohn, L. A.; Christiansen, P. A. *J. Chem. Phys.* **1990**, *93*, 6654.
(31) Krebs, B.; Hasse, K. D. *Acta Crystallogr.* **1976**, *32B*, 1334.
(32) Chen, H.; Kraskowski, M.; Fitzgerald, G. *J. Chem. Phys.* **1993**, *98*, 8710.
(33) Troullier, N.; Martins, J. L. *Phys. Rev. B* **1991**, *43*, 1993.
(34) Weinstock, N.; Schulze, H.; Müller, A. *J. Chem. Phys.* **1973**, *59*, 5063.

Table 6. Predicted LDFT Vibrational Frequencies for $MO_2F_2^+$ and MO_4^- (M = Tc, Re)[a]

	expt, TcO_2F_3·PnF_5 adduct		free $TcO_2F_2^+$		free *cis*-$TcO_2F_2(FH)_2^+$		
symm	As/Sb[g] HF soln	As/Sb[h] solid	all-electron[c]	HW[d]	EC[e]	all-electron[c]	assignt
A_1	992/993	997/995	1034 (35)	1050 (32)	1056 (31)	1016 (57)	$\nu_s(TcO_2)$
	701/680	720/721	757 (42)	759 (43)	762 (44)	705 (26)	$\nu_s(TcF_2)$
	409/407	414/410	374 (0)	383 (0)	385 (0)	380 (23)	$\delta_{sc}(TcO_2)$
		232/230	189 (4)	200 (5)	197 (5)	224 (1) + 303 (0)[i]	$\delta_{sc}(TcF_2)$
A_2	295/296	295/291	250 (0)	262 (0)	269 (0)	286 (0)	$\delta(OTcF)/\rho_t(TcO_2)$
B_1	972/981	982/977	1035 (59)	1046 (59)	1052 (61)	1019 (108)	$\nu_{as}(TcO_2)$
	234/239	249/244	237 (5)	240 (4)	242 (6)	252 (21) + 303 (0)[i]	$\rho_w(TcF_2)$
B_2		.../746	801 (88)	802 (93)	806 (94)	771 (160)	$\nu_{as}(TcF_2)$
	321/321	319/328	272 (4)	281 (4)	292 (4)	314 (13)	$\rho_w(TcO_2)$

	expt, ReO_2F_3·PnF_5 adduct		free $ReO_2F_2^+$			free *cis*-$ReO_2F_2(FH)_2^+$	
symm	As/Sb[g] HF soln	As/Sb[h] solid	PP[f]	HW[d]	EC[e]	EC[e]	assignt
A_1	1037/1035	1035/1040	1058 (16)	1076 (18)	1081 (19)	1060 (41)	$\nu_s(ReO_2)$
	701/689	727/718	778 (42)	771 (43)	773 (44)	735 (25)	$\nu_s(ReF_2)$
	404/403	404/407	397 (0)	378 (0)	378 (0)	388 (48)	$\delta_{sc}(ReO_2)$
	.../223	201/...	236 (3)	208 (3)	209 (3)	208 (1) + 293 (0)[i]	$\delta_{sc}(ReF_2)$
A_2	293/289	291/294	314 (0)	276 (0)	277 (0)	296 (0)	$\delta(OReF)/\rho_t(ReO_2)$
	1012/1011	1009/1019	1032 (52)	1056 (57)	1060 (58)	1042 (96)	$\nu_{as}(ReO_2)$
	236/239	236/237	262 (4)	227 (4)	228 (4)	231 (19) + 296 (0)[i]	$\rho_w(ReF_2)$
B_2	740/...		793 (75)	787 (80)	788 (81)	762 (138)	$\nu_{as}(ReF_2)$
	325/321	322/324	335 (3)	288 (0)	279 (3)	313 (14)	$\rho_w(ReO_2)$

	TcO_4^-				ReO_4^-			
symm	expt[b]	all-electron[c]	HW[d]	EC[e]	expt[b]	PP[f]	HW[d]	EC[e]
A	912	905 (0)	923 (0)	929 (0)	971	953 (0)	965 (0)	969 (0)
E	325	307 (0)	312 (0)	313 (0)	331	374 (0)	323 (0)	324 (0)
T_1	912	922 (665)	932 (678)	937 (683)	920	911 (655)	926 (656)	928 (662)
	336	326 (16)	326 (18)	328 (18)	331	332 (16)	309 (23)	310 (23)

[a] Vibrational frequencies are in cm^{-1}, and values in parentheses are infrared intensities in km mol^{-1}. [b] Reference 34. [c] All-electron calculation with DZVP basis set. [d] Hay−Wadt ECP (refs 26−28) + DZVP2 basis set. [e] Ermler−Christiansen ECPs (refs 29, 30) + DZVP2 basis set. [f] PP (refs 32,33) + DZVP2. [g] Average values taken from Table 4. [h] Average values taken from Table 3. [i] Minor contribution.

distances of 2.32 [2.34 (rhenium values in square brackets)] Å and an (H)F_b---M---F_b(H) angle of 78.8 [78.1]°. The complex was fully optimized to C_{2v} symmetry, which resulted in two imaginary frequencies corresponding to the HF groups moving in and out of the plane. These geometries should, however, provide a reasonable representation of what is occurring in the first coordination sphere of the metal. Coordination of the HF molecules causes the M−O and M−F bonds to lengthen relative to those in free $MO_2F_2^+$. The biggest change is in the F−M−F angle, which increases from 116 [118] to 138 [138]°. However, the geometry clearly is not an ideal octahedron, with the F−M−F angle being closer to the tetrahedral angle than to 180° for the octahedron.

The LDFT geometries and vibrational frequencies calculated for the *cis*-dioxo HF adducts of both $MO_2F_2^+$ cations are in the best overall agreement with the experimental values for the solid SbF_5 adducts of MO_2F_3 and for the PnF_5 adducts in PnF_5-acidified HF solutions. As in the case of the experimental M---F_b bridge distances in the SbF_5 adducts (see X-ray Crystal Structures of TcO_2F_3·SbF_5 and ReO_2F_3·SbF_5), the calculated M---F_b bridge distances of the HF adducts of $MO_2F_2^+$ are similar to each other and reflect the stronger Lewis acid character of ReO_2F_3. The calculated M---F_b distances are both significantly longer than those in the SbF_5 adducts, and this is in accord with the anticipated greater fluoride ion affinity of H^+ relative to that of SbF_5.

The vibrational spectra for the isolated $MO_2F_2^+$ ions agree reasonably well with the experimental results except for the M−F stretches and bends. For the stretches, the isolated ion spectra predict higher values than observed whereas the FMF bends are predicted to be too low. Addition of the two HF molecules significantly improves the agreement with experiment. The M−O stretches exhibit a slight decrease whereas the M−F symmetric stretch exhibits a significant decrease. The FMF bend shows a significant increase on complexation, and we note that it contributes to two modes with the higher one in good agreement with experiment. The OMO bend is essentially unchanged on complexation, but the OMO out-of-plane bend increases to give better agreement with experiment. Complexation has a greater impact on the MF_2 moiety and is consistent with the geometry changes on complexation. The asymmetric (H)F_b−M stretch is predicted to be at 303 [296] cm^{-1} with a contribution to the MF_2 out-of-plane bending mode at 252 [231] cm^{-1}. The symmetric (H)F_b---M stretch is predicted to be at 303 [293] cm^{-1}, and the (H)F_b---M---F_b(H) bend is predicted to be at 70 [64] cm^{-1}.

The $ReO_2F_2(CH_3CN)_2^+$ Cation. (a) NMR Spectroscopy. The ^{19}F NMR spectrum of ReO_2F_3·SbF_5 dissolved in CH_3CN at 0 °C consists of a multiplet at −122.8 ppm resulting from the superposition of an equiintense sextet and an equiintense octet (relative integrated intensities 1.00:2.85) arising from the SbF_6^- anion [$^1J(^{19}F-^{121}Sb)$ = 1932 Hz; $^1J(^{19}F-^{123}Sb)$ = 1044 Hz], in excellent agreement with the literature values for [Ag]-[SbF_6] in CH_3CN [−123 ppm; $^1J(^{19}F-^{121}Sb)$ = 1934 Hz; $^1J(^{19}F-^{121}Sb)$ = 1047)][35] and a singlet at 7.2 ppm ($\Delta\nu_{1/2}$ = 15 Hz) assigned to F on Re^{VII}. The well-resolved spin−spin couplings between ^{19}F and the quadrupolar ^{121}Sb and ^{123}Sb nuclei and relative intensities of the F-on-Re^{VII} and F-on-Sb^V

(35) Kidd, R. G.; Matthews, R. W. *Inorg. Chem.* **1972**, *11*, 1156.

resonances (3:1) indicate dissociation of the adduct into distinct cations and anions. The $ReO_2F_2^+$ cation is expected to be highly acidic and to coordinate to two solvent molecules in order to achieve a coordination number of 6. The occurrence of a sharp singlet in the ^{19}F NMR spectrum indicates that the two fluorine ligands are symmetry equivalent. The ^1H NMR spectrum consists of two singlets at 2.00 and 2.64 ppm, corresponding to the solvent and a single chemical environment for complexed CH_3CN, respectively. The ^{13}C NMR spectrum also shows a single chemical environment for complexed CH_3CN at 125.4 (CN) and 3.10 ppm (CH_3), as well as the solvent at 117.4 (CN) and 0.48 (CH_3) ppm. The complexation shifts for $ReO_2F_2(CH_3CN)_2^+$ (0 °C; $\Delta\delta(^1H) = 0.64$ ppm; $\Delta\delta(^{13}CH_3) = 2.62$ ppm; $\Delta\delta(^{13}CN) = 8.00$ ppm) are significantly larger than those observed for $ReO_2F_3(CH_3CN)$ in SO_2ClF solvent (−80 °C; $\Delta\delta(^1H) = 0.46$ ppm; $\Delta\delta(^{13}CH_3) = 1.08$ ppm; $\Delta\delta(^{13}CN) = 1.54$ ppm).[12] These observations are consistent with two symmetry-equivalent CH_3CN ligands and the greater Lewis acidity of the $ReO_2F_2^+$ cation relative to that of ReO_2F_3. The arrangement of the oxygens in the complex is expected to be cis, as in all d^0 dioxo−transition metal complexes, and the CH_3CN ligands are expected to coordinate to the positions trans to the oxo ligands, as observed for $MoO_2F_2(thf)_2$,[36] $MOF_4(CH_3CN)$ (M = Mo, W),[37] $MO_2F_3(CH_3CN)$ (M = Tc,[11] Re[12]), and $ReO_3F(CH_3CN)_2$.[12] As a result, the ligand arrangement inferred for the $ReO_2F_2(CH_3CN)_2^+$ cation is shown in structure **III**.

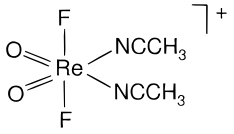

Structure III

Acetonitrile solutions of $[ReO_2F_2(CH_3CN)_2][SbF_6]$ slowly decomposed at 0 °C, with the original colorless solution turning dark red within ca. 20 min. As the decomposition proceeded, a doublet and a triplet [$^1J(^{19}F-^{19}F) = 117$ Hz] appeared at −24.6 and −33.1 ppm, respectively, arising from the colorless $ReO_2F_3(CH_3CN)$ adduct. The low solubility of the $[ReO_2F_2(CH_3CN)_2][SbF_6]$ salt in CH_3CN prevented the acquisition of NMR spectra at temperatures lower than 0 °C, and no attempt was made to identify the species responsible for the intense dark red color.

(b) Raman Spectroscopy. The Raman spectrum of $[ReO_2F_2(CH_3CN)_2][SbF_6]$ isolated from CH_3CN solution is shown in Figure 5. The observed frequencies and their assignments for the cation (C_{2v} point symmetry) and the anion (O_h point symmetry) are listed in Table 7. The vibrational assignments were made by comparison with the Raman spectra of polymeric ReO_2F_3,[12] $ReO_2F_3{\cdot}PnF_5$ (Tables 3 and 4), $ReO_2F_3(CH_3CN)$,[12] CH_3CN,[38,39] and $ReO_2F_4^-$ [12] and by comparison with the calculated values for the $ReO_2F_2^+$ and *cis*-$ReO_2F_2(FH)_2^+$ cations (Table 6).

The antisymmetric and symmetric ReO_2 stretching modes are readily assigned to bands at 998 and 1012 cm^{-1}, respectively, and their presence confirms the *cis*-dioxo arrangement predicted for the cation (see NMR Spectroscopy). The antisymmetric and symmetric ReF_2 stretching modes occur at 574 and 648 cm^{-1}, respectively, and display an ordering which is opposite to that for the $MO_2F_3{\cdot}PnF_5$ adducts but the same as that for $TcO_2F_4^-$

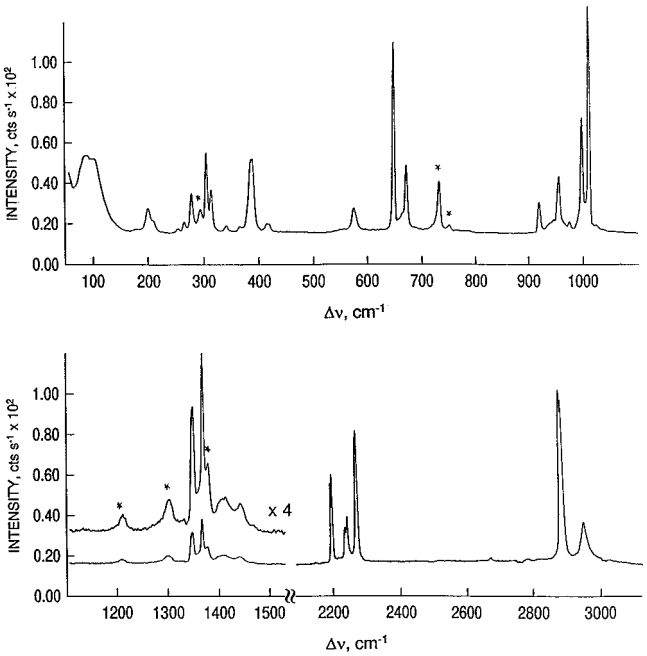

Figure 5. Raman spectrum of microcrystalline $[ReO_2F_2(CH_3CN)_2][SbF_6]$ recorded in FEP at −150 °C using 514.5-nm excitation. Asterisks (∗) denote FEP sample tube lines.

Table 7. Raman Frequencies, Assignments, and Mode Descriptions for $[ReO_2F_2(CH_3CN)_2][SbF_6]$[a]

	assignt[c]	
freq[b] (cm^{-1})	$ReO_2F_2(CH_3CN)_2^+$ (C_{2v})	SbF_6^- (O_h)
3012 (21)	$\nu_{as}(CH_3)$	
2950 (86), sh	$\nu_s(CH_3)$	
2330 (71), 2327 (66), sh	ν(CN)	
1448 (3)	$\delta_{as}(CH_3)$	
1411 (3)	$\delta_{as}(CH_3)$	
1355 (13)	$\delta_s(CH_3)$	
1012 (100)	B_1, $\nu_{as}(ReO_2)$	
998 (49)	ν(CC)	
956 (24)		
672 (29)		A_{1g}, $\nu_s(SbF_6)$
648 (82)	A_1, $\nu_s(ReF_2)$	
574 (10)	B_2, $\nu_{as}(ReF_2)$	
558 (1)		E_g, $\nu_{as}(SbF_4)$
419 (4)	δ(CCN)	
414 (4)	δ(CCN)	
388 (32)	A_1, $\delta(ReO_2)$	
365 (3), 340 (3)	*d*	
313 (19)	A_1, $\delta(ReF_2)$	
304 (35)	B_2, $\rho_w(ReO_2)$	
293 (15)	B_1, $\delta(ReF_2)$	
277 (17)	A_2, $\rho_t(ReO_2)$	T_{2g}, $\delta_s(SbF_4)$
264 (5)	A_1, $\nu_s(ReN_2)$	
253 (2)	B_1, $\delta_{as}(ReN_2)$	
209 (5), sh	*d*	
199 (10)	B_2, $\rho_w(ReN_2)$	
177 (1)	*d*	
101 (22)	A_1, $\delta(ReN_2)$	
86 (19)	B_1, $\rho_t(ReO_2)$	
54 (5)	A_2, $\rho_t(ReN_2)$	

[a] The spectrum was recorded on the microcrystalline solid in FEP at −150 °C using 514.5-nm excitation. Bands assigned to residual CH_3CN solvent (C_{3v} point symmetry): $\nu_1(A_1)$, 2945 (90), $2\nu_3$, 2730 (1); $\nu_3 + \nu_4$, 2293 (21), 2300 (24), $\nu_2(A_1)$, 2252 (45), 2256 (48), $\nu_3(A_1)$, 1374 (16), $\nu_4(A_1)$, 919 (12). [b] Abbreviations are defined in Table 3, footnote *a*. [c] Symbols are defined in Table 3, footnote *b*. [d] Unassigned band.

(36) Rhiel, M.; Wocadlo, S.; Massa, W.; Dehnicke, K. *Z. Anorg. Allg. Chem.* **1996**, *622*, 1195.
(37) Buslaev, Y. A.; Kokunov, Y. V.; Bochkareva, V. A.; Shostorovich, E. M. *Russ. J. Inorg. Chem. (Engl. Transl.)* **1972**, *17*, 1675; *Zh. Neorg. Khim.* **1972**, *17*, 3184.
(38) Günthard, H. H.; Kováts, E. *Helv. Chim. Acta* **1952**, *145*, 1190.
(39) Yamadera, R.; Kremm, S. *Spectrochim. Acta* **1968**, *24A*, 1677.

and for $ReO_2F_4^-$. The band at 388 cm^{-1} is assigned to the ReO_2 scissoring motion, which is at lower frequency than those for ReO_2F_3 (412 cm^{-1}), $ReO_2F_3 \cdot SbF_5$ (407 cm^{-1}), and $ReO_2F_3(CH_3CN)$ (408 cm^{-1}). The remaining low-frequency bands are very similar to those in the $ReO_2F_3 \cdot SbF_5$ spectrum and are tentatively assigned to ReF_2 bending motions as well as to ReO_2 and ReN_2 wagging, twisting, and rocking motions. The antisymmetric and symmetric ReN_2 stretching modes are expected to occur in the 200−300 cm^{-1} region of the spectrum as observed for other transition metal complexes with CH_3CN[38] and are tentatively assigned to the bands at 253 and 264 cm^{-1}, respectively. The Raman-active $\nu_1(A_g)$, $\nu_2(E_g)$, and $\nu_5(T_{2g})$ modes associated with the octahedral SbF_6^- anion are in good agreement with the values previously reported in the literature[24] and are consistent with an SbF_6^- anion that is not significantly distorted from O_h symmetry. The bands assigned to ν_8 (378 cm^{-1}), ν_4 (920 cm^{-1}), ν_6 (1448 cm^{-1}), and $\nu_3 + \nu_4$ (2297 cm^{-1}) of free CH_3CN are shifted to 414/419, 956, 1411, and 2327/2330 cm^{-1}, respectively, in $[ReO_2F_2(CH_3CN)_2][SbF_6]$ and are similar to those observed for $ReO_2F_3(CH_3CN)$,[12] $TcO_2F_3(CH_3CN)$,[11] and alkali, alkaline earth, and transition metal complexes such as the $Co(CH_3CN)_6^{2+}$ cation.[40,41]

The $TcO_2F_3 \cdot XeO_2F_2$ Adduct. Xenon hexafluoride is used in the preparation of TcO_2F_3 to scavenge water produced by the solvolysis of Tc_2O_7 in HF and to fluorinate TcO_3F to TcO_2F_3 (eqs 4−6).[13] The stoichiometry for the complete conversion of

$$Tc_2O_7 + 4\,HF \rightarrow 2TcO_3F + H_3O^+ + HF_2^- \quad (4)$$

$$XeF_6 + H_3O^+ + HF_2^- \rightarrow XeOF_4 + 4HF \quad (5)$$

$$TcO_3F + XeF_6 \rightarrow TcO_2F_3 + XeOF_4 \quad (6)$$

Tc_2O_7 to TcO_2F_3 and formation of $XeOF_4$ corresponds to the molar ratio XeF_6:Tc_2O_7 = 3:1. When smaller quantities of XeF_6 are used (a 1.5:1 molar ratio was used in the present work), $XeOF_4$ acts as a fluorinating agent and XeO_2F_2 is formed (eq 7). The pale yellow adduct $TcO_2F_3 \cdot XeO_2F_2$ was sublimed from

$$TcO_3F + XeOF_4 \rightarrow TcO_2F_3 + XeO_2F_2 \quad (7)$$

a mixture of TcO_2F_3 and $TcO_2F_3 \cdot XeO_2F_2$ under static vacuum at 45 °C and showed no sign of decomposition when stored under dry nitrogen at room temperature for at least 2 weeks.

(a) X-ray Crystal Structure of $TcO_2F_3 \cdot XeO_2F_2$. Details of the data collection parameters and other crystallographic information are given in Table 1 and in the Supporting Information. Important bond lengths, bond valences, and bond angles and significant long contacts are listed in Table 2.

The structure of $TcO_2F_3 \cdot XeO_2F_2$ consists of infinite chains of TcO_2F_3 running parallel to the *c* axis and bridged to XeO_2F_2 chains by long Tc−F···Xe contacts (Figure S2 (Supporting Information)). There is one O···O contact between the TcO_2F_3 chains (O(1)···O(2), 2.781 Å) and one O···F contact between a TcO_2F_3 chain and XeO_2F_2 (O(2)···F(3), 2.799 Å) which are at the limit of the sum of the van der Waals radii of F and O.[9,10]

The Tc atoms in the TcO_2F_3 chains are bonded to two oxygens that are cis to each other (Figure 6a) and trans to the bridging fluorines and two fluorine atoms that are cis to the oxygens and trans to each other, as was observed in the crystal

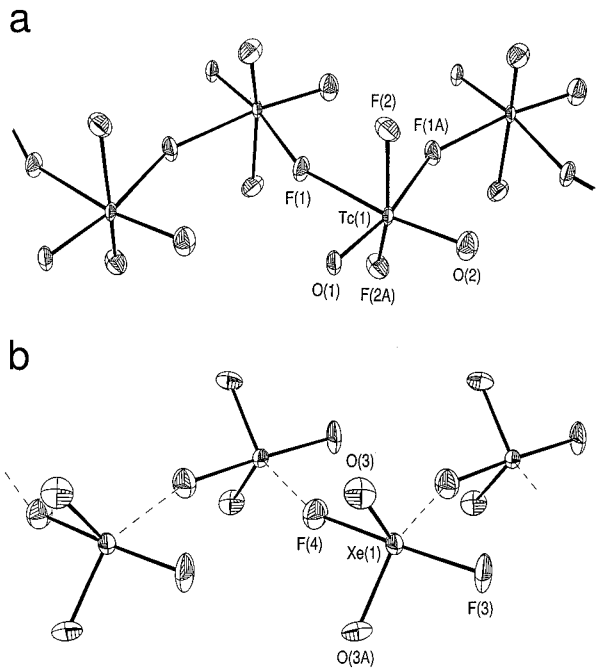

Figure 6. Structures of (a) the TcO_2F_3 infinite chain and (b) the XeO_2F_2 infinite chain portions of the $TcO_2F_3 \cdot XeO_2F_2$ adduct. Thermal ellipsoids are shown at the 50% probability level.

structure of TcO_2F_3.[13] All bond lengths and bond angles are identical (within 3σ) to those reported previously for polymeric TcO_2F_3.

The arrangement of the light atoms around Xe is similar to what was observed in the structure of XeO_2F_2 and is consistent with the disphenoidal AX_2Y_2E geometry predicted by the VSEPR model;[15] i.e., the doubly bonded oxygen atoms and the lone pair occupy the equatorial plane and the fluorine atoms lie in axial positions. An interesting feature of this structure is that the XeO_2F_2 molecules have secondary contacts to Xe through fluorine bridging within the XeO_2F_2 chains (Figure 6b), rather than through Xe···O contacts as in the structure of XeO_2F_2.[42] The Xe−O distance (1.734(9) Å) is equal (within 3σ) to that in XeO_2F_2 (1.714(4) Å) and similar to the Xe=O bond lengths of $XeOF_4$ (1.706(15),[43] 1.708(2),[44] 1.711(3)[45] Å) and XeO_3 (1.76(3) Å).[46] There are two types of axial Xe−F bonds in the present structure. One is slightly longer (1.925(13) Å) than the other (1.892(13) Å) as a result of a secondary fluorine bridge contact with Xe in a neighboring XeO_2F_2 molecule, and both agree well with the Xe^{VI}−F bond lengths previously reported for XeO_2F_2 (1.899(3) Å)[42] and $XeOF_4$ (1.903(5),[43] 1.9024(9),[44] 1.892(2)[45] Å). All bond angles are identical to those in XeO_2F_2. Contrary to the VSEPR model prediction, the F−Xe−F angle is bent *toward* the nonbonding electron pair on xenon both in the present structure and in the structure of XeO_2F_2. This feature was also observed in the X-ray structures of XeO_2F_2[42] and $XeO_2(OTeF_5)_2$,[47] as well as in the gas phase (microwave[43] and electron diffraction[44]) structures of $XeOF_4$. Huston and co-workers[42] explained this feature in

(40) Reedijk, J.; Groeneveld, W. L. *Recl. Trav. Chim. Pays-Bas* **1968**, *87*, 1079.
(41) Reedijk, J.; Zuur, A. P.; Groeneveld, W. L. *Recl. Trav. Chim. Pays-Bas* **1967**, *86*, 1127.
(42) Peterson, S. W.; Willett, R. D.; Huston, J. L. *J. Chem. Phys.* **1973**, *59*, 453.
(43) Martins, J. F.; Wilson, E. B. *J. Mol. Spectosc.* **1968**, *26*, 410.
(44) Jacob, E. J.; Thompson, H. B.; Bartell, L. S. *J. Mol. Struct.* **1971**, *8*, 383.
(45) Pointner, B. E.; Schrobilgen, G. J. Unpublished results.
(46) Templeton, D. H.; Zalkin, A.; Forester, J. D.; Williamson, S. M. In *Noble Gas Compounds*; Hyman, H. H., Ed.; University of Chicago: Chicago, IL,1963; p 221.
(47) Turowsky, L.; Seppelt, K. *Z. Anorg. Allg. Chem.* **1992**, *609*, 153.

Table 8. Raman Frequencies, Assignments, and Mode Descriptions for the $TcO_2F_3 \cdot XeO_2F_2$ Adduct[a]

	assignt[c]		freq (cm^{-1})	
freq[b] (cm^{-1})	TcO_2F_4 (C_{2v})[e]	XeO_2F_2 (C_{2v})[f]	XeO_2F_2[d] solid (C_{2v})	XeO_2F_2[d] matrix (C_{2v})
984 (84)	A_1, $\nu_s(TcO_2)$			
959 (26)	B_1, $\nu_{as}(TcO_2)$			
889 (3)		B_1, $\nu_{as}(XeO_2)$	881 (39)	906, s
840 (100)		A_1, $\nu_s(XeO_2)$	853 (100)	849, mw
633 (30)	A_1, $\nu_s(TcF_2)$			
620 (5), sh	B_2, $\nu_{as}(TcF_2)$			
580 (2), br	A_1, $\nu_s(TcF_{2b})$			
559 (5), sh	B_1, $\nu_{as}(TcF_{2b})$			
553 (8)		B_2, $\nu_{as}(XeF_2)$	578 (>1)	585, vs
499 (28)		A_1, $\nu_s(XeF_2)$	537 (33)	537, w
426 (11); 422 (6), sh	A_1, $\delta_{sc}(TcO_2)$			
343 (17)		A_1, $\delta_{sc}(XeO_2)$	344 (2.5)	331, sh
336 (10), sh; 334 (12)	B_2, $\rho_w(TcO_2)$			
		A_2, $\tau(XeO_2)$	318 (~1)	329, sh
307 (28)		B_2, $\delta_{rock}(XeO_2)$	314 (6)	324, m
284 (32)	A_2, $\rho_t(TcO_2)$			
268 (10)	B_1, $\rho_w(TcF_2)$			
		B_1, $\delta_{sc}(XeF_2)$	222 (1.2)	
209 (1)		A_1, $\delta_{sc}(XeF_2)$	202 (1.4)	202, w
195 (3)	A_1, $\delta_{sc}(TcF_{2b})$			
152 (1), 129 (2), 111 (2), 94 (<1), 74 (3)	unassigned deformation and lattice modes			

[a] The spectrum was recorded on microcrystalline solid in FEP at 23 °C using 514.5-nm excitation. [b] Values in parentheses denote relative Raman intensities. Abbreviations are defined in Table 3, footnote *a*. [c] Symbols are defined in Table 3, footnote *b*. [d] Reference 58. [e] The vibrational modes of the TcO_2F_4 units (point symmetry C_{2v}) belong to the irreducible representations $6A_1 + 2A_2 + 4B_1 + 3B_2$ (the [O, O, Tc, F_b, F_b] plane is taken as the $\sigma_v(xz)$ plane with the *z* axis as the principal axis) and are all Raman active whereas only the A_1, B_1, and B_2 modes are infrared active. [f] The vibrational modes of the XeO_2F_2 units (point symmetry C_{2v}) belong to the irreducible representations $4A_1 + A_2 + 2B_1 + 2B_2$ and are all Raman active whereas the A_1, B_1, and B_2 modes are infrared active.

the structure of XeO_2F_2 by assuming that the Xe−O double bonds repel the Xe−F bonds more effectively than the Xe lone pair, whereas the small O−Xe−O angle results from an inherent preference of the oxygen ligands to bond to the Xe p orbitals rather than to the Xe s orbital, and not because of repulsion from the lone valence electron pair on Xe. Gillespie and Robinson[48] explain these apparent inconsistencies by assuming that the lone-pair domain exerts directional repulsive effects; i.e., a lone-pair domain in an equatorial position spreads out more in the equatorial direction than in the axial direction.

The total bond valence for the technetium atom is 7.08 vu, with contributions of 2.06 vu/oxygen atom, 0.97 vu/terminal fluorine atom, and 0.52 vu/bridging fluorine atom, which are essentially identical to those calculated for polymeric TcO_2F_3.[13] The total bond valence for the xenon atom is 6.02 vu, with contributions of 1.79 vu/oxygen atom and 0.91 vu/terminal fluorine atom. The coordination sphere around Xe is completed by one long contact with a terminal fluorine of another XeO_2F_2 unit (2.985(13) Å, 0.20 vu) and two terminal fluorines of the TcO_2F_3 chain (2.848(8) Å, 0.23 vu) (vide supra). The long contacts between Xe and the terminal fluorine atoms on Tc are significantly shorter than the sum of the van der Waals radii (3.63 Å),[10] as indicated by their bond valence values (0.23 vu), and clearly indicate that XeO_2F_2 is acting as a fluoride ion acceptor toward TcO_2F_3. This Lewis acid−base interaction, in which the TcO_2F_3 chain is only slightly perturbed, is significantly weaker than that in the $TcO_2F_3 \cdot SbF_5$ adduct, in which the SbF_5 is incorporated directly into the TcO_2F_3 chain, and is consistent with the significantly stronger Lewis acid character of SbF_5 relative to that of XeO_2F_2. It is also noteworthy that the three long Xe···F contacts are directed so that they avoid the valence lone pair of the xenon atom, as observed in the structures of XeF_3^+,[49−51] XeF_5^+,[52−56] and $XeOF_3^+$ [57] salts.

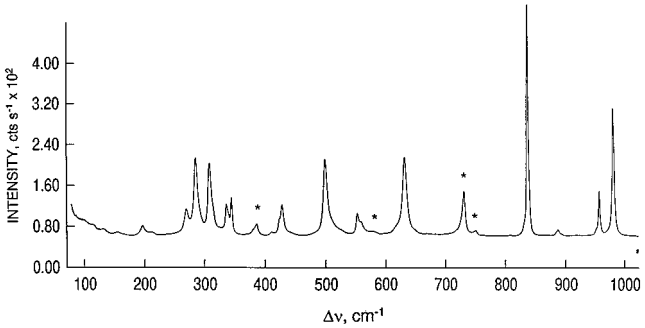

Figure 7. Raman spectrum of $TcO_2F_3 \cdot XeO_2F_2$ recorded in FEP at 23 °C using 514.5-nm excitation. Asterisks (∗) denote FEP sample tube lines.

(b) Raman Spectrum of $TcO_2F_3 \cdot XeO_2F_2$. The Raman spectrum of the $TcO_2F_3 \cdot XeO_2F_2$ adduct is shown in Figure 7, and the vibrational frequencies and their assignments are listed in Table 8. Vibrational assignments for the adduct are largely based on correlations with the Raman spectra of polymeric TcO_2F_3,[13] $TcO_2F_4^-$,[11] and $TcO_2F_3 \cdot PnF_5$ (Tables 3 and 4) calculated values for $TcO_2F_4(FH)_2^+$ (Table 6) and XeO_2F_2.[58]

(48) Gillespie, R. G.; Robinson, E. A. *Angew. Chem., Int. Ed. Engl.* **1996**, *35*, 495; *Angew. Chem.* **1996**, *108*, 539.
(49) Boldrini, P.; Gillespie, R. J.; Ireland, P. R.; Schrobilgen, G. J. *Inorg. Chem.* **1974**, *13*, 1690.
(50) McKee, D. E.; Zalkin, A.; Bartlett, N. *Inorg. Chem.* **1973**, *12*, 1713.
(51) Gillespie, R. J.; Martin, D.; Schrobilgen, G. J. *J. Chem. Soc., Dalton Trans.* **1977**, 2234.
(52) Adams, C. J.; Bartlett, N. *Isr. J. Chem.* **1978**, *17*, 114.
(53) Bartlett, N.; Gennis, M.; Gibler, D. D.; Morrell, B. K.; Zalkin, A. *Inorg. Chem.* **1973**, *12*, 1717.
(54) Bartlett, N.; Einstein, F.; Stewart, D. F.; Trotter, J. *J. Chem. Soc., Chem. Commun.* **1966**, 550.
(55) Bartlett, N.; Einstein, F.; Stewart, D. F.; Trotter, J. *J. Chem. Soc. A* **1967**, 1190.
(56) Frlec, B.; Bohinc, M.; Charpin, P.; Drifford, M. *J. Inorg. Nucl. Chem.* **1972**, *34*, 2938.
(57) Mercier, H. P. A.; Sanders, J. C. P.; Schrobilgen, G. J.; Tsai, S. S. *Inorg. Chem.* **1993**, *32*, 386.
(58) Christe, K. O.; Wilson, W. W. *Inorg. Chem.* **1988**, *27*, 3763.

A number of deformation modes associated with XeO_2F_2 (XeO_2 twist, XeO_2 wag, and out-of-plane XeF_2 bend) were not observed but are expected to be very weak on the basis of the intensities reported for XeO_2F_2 (see Table 8).

The symmetric and antisymmetric Tc−O stretches are assigned to bands at 984 and 959 cm^{-1}, respectively, and occur at higher frequency compared to the corresponding stretches for polymeric TcO_2F_3 (974 and 963 cm^{-1}), which is consistent with the increased valence bond orders observed in the crystal structure of $TcO_2F_3 \cdot XeO_2F_2$ and the fluoride ion donor properties of TcO_2F_3 in this adduct. The preference for fluorine bridge (Xe···F secondary contact) formation within XeO_2F_2 chains in $TcO_2F_3 \cdot XeO_2F_2$ (see X-ray Crystal Structure of $TcO_2F_3 \cdot XeO_2F_2$) versus oxygen bridge (Xe···O secondary contact) formation in solid XeO_2F_2 is not unambiguously reflected in their relative Xe−F and Xe−O stretching frequencies (Table 8). The $\nu_{as}(XeO_2)$ modes of solid XeO_2F_2 (881 cm^{-1}) and of the adduct (889 cm^{-1}) exhibit the expected trend and are significantly lower than those for matrix-isolated XeO_2F_2 (906 cm^{-1}), where no short Xe···F or Xe···O contacts can occur. Although the $\nu_s(XeO_2)$ stretches show no consistent trend, the symmetric and antisymmetric Xe−F stretches at 499 and 553 cm^{-1} for the adduct display significant shifts to lower frequency relative to those of solid XeO_2F_2 (537 and 578 cm^{-1}) and matrix-isolated XeO_2F_2 (537 and 585 cm^{-1}) that likely arise from Xe···F interactions in the adduct. The stretching frequencies for XeO_2F_2 in the adduct are generally intermediate between those of pure XeO_2F_2 and the $XeO_2F_3^-$ anion[58,59] and reflect the more polar nature of the XeO_2F_2 bonding in the adduct and the Lewis acid behavior of XeO_2F_2 toward TcO_2F_3 in this adduct; they are also consistent with Tc−F···Xe secondary interactions found in the crystal structure of $TcO_2F_3 \cdot XeO_2F_2$.

Conclusion

Both TcO_2F_3 and ReO_2F_3 were shown to behave as fluoride ion donors toward the strong fluoride ion acceptors AsF_5 and SbF_5. Although discrete $TcO_2F_2^+$ and $ReO_2F_2^+$ cations could not be definitively characterized in PnF_5-acidified HF and SbF_5 solutions by NMR and Raman spectroscopy, the spectroscopic findings are consistent with the formation of solvated $MO_2F_2^+$ cations such as *cis*-$MO_2F_2(FH)_2^+$. Although the solution structures of the cations could not be firmly established because of lack of detail in the vibrational and NMR spectra, the assumptions are reasonable and are supported by theoretical calculations. The high solubilities of the $MO_2F_3 \cdot PnF_5$ adducts in HF and the characterization of $[ReO_2F_2(CH_3CN)_2][SbF_6]$ in CH_3CN solutions of $ReO_2F_3 \cdot SbF_5$ also support these findings. In the solid state, the $MO_2F_3 \cdot PnF_5$ adducts show strong interactions through the formation of strong fluorine bridges and adduct structures comprising of chains of alternating fluorine-bridged MO_2F_4 and PnF_6 units. In contrast, $TcO_2F_3 \cdot XeO_2F_2$ only shows weak interactions in the form of long fluorine atom contacts between XeO_2F_2 and the TcO_2F_3 chains. In each case, the *cis*-dioxo arrangement around the transition metal is maintained and bridging always occurs trans to the oxygen ligands. The $ReO_2F_3 \cdot SbF_5$ adduct undergoes dissociation and self-association in SO_2ClF solvent to give the fluorine-bridged binuclear $Re_2O_4F_5^+$ cation, a rare example of a five-coordinate transition metal oxofluoride.

Experimental Section

All operations were conducted in laboratories that were monitored routinely by the McMaster University Health Physics Group for radioactive contamination. All work involving ^{99}Tc was licensed and performed according to the regulations and recommendations of the Canadian Atomic Energy Control Board.[60]

Apparatus and Materials. Volatile materials were handled in vacuum lines constructed of nickel, stainless steel, FEP, and Pyrex, and nonvolatile materials were handled in the dry nitrogen atmosphere of a drybox as previously described.[13] ***Caution!*** Anhydrous HF must be handled using appropriate protective gear with immediate access to proper treatment procedures in the event of contact with the liquid or vapor. Solid residues and HF solutions containing XeO_2F_2 may hydrolyze in air to form highly shock-sensitive and explosive XeO_3. Such residues and all other HF solutions were disposed of by slowly pouring the cold solid or the cold HF solution (−78 °C) into a mixture of ice and NaOH solution inside a fume hood.

The methods for the preparation of TcO_2F_3,[13] ReO_2F_3,[12] AsF_5,[57] and XeF_6[61] have been described previously. Antimony trifluoride (Aldrich, 98%) was sublimed under dynamic vacuum at ca. 200 °C prior to use. Fluorine gas (Air Products) was used without further purification. The solvents, CH_3CN[62] (HPLC Grade, Caledon Laboratories Ltd.), SO_2ClF[63] (Columbia Organic Chemical Co.), HF[64] (Harshaw Chemical Co.), and SbF_5[65] (Ozark-Mahoning Co.), were dried/purified by the standard literature methods.

$TcO_2F_3 \cdot SbF_5$ and $ReO_2F_3 \cdot SbF_5$. The preparation of $ReO_2F_3 \cdot SbF_5$ was similar to that of $TcO_2F_3 \cdot SbF_5$ except where indicated in brackets. In typical preparations and in the drybox, 0.0737 g (0.392 mmol) of TcO_2F_3 [0.0997 g (0.362 mmol) of ReO_2F_3] and 0.0783 g (0.438 mmol) [0.0653 g (0.365 mmol)] of SbF_3 were loaded into the vertical and horizontal arms, respectively, of a T-shaped reactor constructed from three lengths of $^1/_4$-in-o.d. FEP tubing, two of which (each ca. 20 cm in length) were heat-sealed at one end and connected through a PTFE Swagelok T-piece while the remaining shorter length (ca. 7 cm) was fitted with a Kel-F valve. Approximately 0.3 mL of HF was condensed onto the SbF_3 and reacted with excess F_2 gas until a clear, colorless solution was obtained (ca. 1 h). The resulting SbF_5/HF solution was then decanted onto TcO_2F_3 [ReO_2F_3], which dissolved upon agitation. The reactor was then evacuated, and the HF and excess SbF_5 were pumped off through an FEP U-trap cooled to −196 °C, yielding a pale yellow [white] solid, which was dried overnight under dynamic vacuum; yield 0.1616 g (0.399 mmol) [0.1721 g (0.350 mmol)]. Single crystals were grown by dissolving 0.1100 g of $TcO_2F_3 \cdot SbF_5$ [0.2483 g of $ReO_2F_3 \cdot SbF_5$] in 0.3 [0.5] mL of HF [SO_2ClF] inside a $^1/_4$-in. FEP reaction tube. Crystals of $TcO_2F_3 \cdot SbF_5$ were grown by pressurizing the reaction tube with ca. 1000 Torr of nitrogen and allowing the HF to slowly diffuse through the walls of the tube for 5 d. The $ReO_2F_3 \cdot SbF_5$ mixture in SO_2ClF was sonicated at 40 °C, and the resulting supernate was decanted into the bent portion of the reaction tube, which was then immersed in a dewar filled with water at 40 °C and left to cool overnight. The supernatant solution was decanted off the pale yellow plates [colorless blocks] that had formed into a depression created by bending the tube, and the remaining solvent was removed under vacuum before transferring the reactor to the drybox. Single crystals were selected under a microscope and individually sealed inside Lindemann capillaries. The crystal used for data acquisition had the dimensions 0.10 × 0.25 × 0.35 [0.20 × 0.25 × 0.31] mm^3.

$TcO_2F_3 \cdot AsF_5$ and $ReO_2F_3 \cdot AsF_5$. The preparation of $ReO_2F_3 \cdot AsF_5$ was similar to that of the Tc analogue except where indicated in brackets. In the drybox, 0.0500 g (0.266 mmol) of TcO_2F_3 [0.1911 g (0.6944 mmol) of ReO_2F_3] was loaded into a 4-mm-o.d. FEP reactor, fitted with a Kel-F valve. Approximately 0.3 mL of HF was distilled into the reactor followed by condensation of AsF_5 (1.20 mmol) [2.40 mmol] from the calibrated manifold of a metal vacuum line onto the frozen solution at −196 °C. The yellow [colorless] solid dissolved

(59) Gillespie, R. J.; Schrobilgen, G. J. *J. Chem. Soc., Chem. Commun.* **1977**, 595.
(60) Atomic Energy Control Board; Radioisotope Safety—Basic Laboratories; INFO-0142-1/Rev. 3; Sept. 5, 1997; AECB: Ottawa.
(61) Chernick, C. L.; Malm, J. G. *Inorg. Synth.* **1966**, *8*, 258.
(62) Winfield, J. M. *J. Fluorine Chem.* **1984**, *25*, 91.
(63) Schrobilgen, G. J.; Holloway, J. H.; Granger, P.; Brevard, C. *Inorg. Chem.* **1978**, *17*, 980.
(64) Emara, A. A. A.; Schrobilgen, G. J. *Inorg. Chem.* **1992**, *31*, 1323.
(65) Gillespie, R. J.; Netzer, A.; Schrobilgen, G. J. *Inorg. Chem.* **1974**, *13*, 1445.

completely upon warming to room temperature with agitation. Hydrogen fluoride and excess AsF_5 were then pumped off at −50 [−45] °C through an FEP U-trap at −196 °C for ca. 8 h [16 h], yielding a pale yellow [white; 0.3001 g (0.6742 mmol)] solid. Samples for NMR analysis were prepared in a manner similar to that described above but were heat-sealed after the addition of AsF_5.

$[ReO_2F_2(CH_3CN)_2][SbF_6]$. In the drybox, 0.0744 g (0.151 mmol) of $ReO_2F_3{\cdot}SbF_5$ was loaded into a 4-mm-o.d. FEP tube fitted with a Kel-F valve. Approximately 0.4 mL of dry CH_3CN was condensed into the reactor at −196 °C, which was then briefly warmed to room temperature (less than 1 min) and sonicated until the solid dissolved. The solvent was then pumped off at −40 °C to yield a white solid, which was maintained at −78 °C until the low-temperature Raman spectrum could be recorded. An NMR sample was prepared by condensing 0.4 mL of CH_3CN onto 0.0251 g (0.0510 mmol) of $ReO_2F_3{\cdot}SbF_5$ at −196 °C. The sample was only warmed to 0 °C immediately before acquisition of the NMR spectrum.

$TcO_2F_3{\cdot}XeO_2F_2$. Approximately 1 mL of anhydrous HF was condensed onto Tc_2O_7 (0.4280 g, 1.1.382 mmol) in a $^1/_4$-in. FEP T-shaped reactor fitted with a Kel-F valve. Two liquid phases formed upon warming at room temperature and vigorous agitation. The mixture was allowed to stand at room temperature for 1 h prior to condensing XeF_6 (0.4234 g, 1.726 mmol) into the reaction tube at −196 °C. A bright yellow precipitate formed upon warming to room temperature, and the supernate over the TcO_2F_3 remained slightly yellow as a consequence of the formation of $[XeF_5][TcO_2F_4]$.[13] The supernate was then decanted into the sidearm of the reactor, and HF was slowly distilled back onto the solid by slowly cooling the vertical tube with liquid nitrogen. The mixture was then agitated and the supernate decanted again into the sidearm. This procedure was repeated five times in an attempt to wash the TcO_2F_3 free of $XeOF_4$ and XeO_2F_2. The sidearm was then heat-sealed and disposed of, and the residual HF was removed from the yellow solid. The lower portion of the reactor was warmed to 45 °C under dynamic vacuum until yellow crystals sublimed, which were identified as $TcO_2F_3{\cdot}XeO_2F_2$ by Raman spectroscopy. The reactor was transferred into the drybox, where single crystals were selected under a microscope and individually sealed inside Lindemann capillaries. The crystal used for the data acquisition had the dimensions $0.05 \times 0.15 \times 0.25$ mm^3.

Crystal Structure Determinations. The crystals were centered on a Syntex $P2_1$ diffractometer, using silver radiation monochromatized with a graphite crystal ($\lambda = 0.560\,86$ Å). The acquisition parameters are given for $TcO_2F_3{\cdot}SbF_5$ followed by those for $ReO_2F_3{\cdot}SbF_5$ in parentheses and $TcO_2F_3{\cdot}XeO_2F_2$ in square brackets. Accurate cell dimensions were determined at 24 (−50) [−100] °C from a least-squares refinement of the setting angles (χ, ϕ, and 2θ) obtained from 22 (15) [20] accurately centered reflections (with $20° \le 2\theta \le 30°$) chosen from a variety of points in reciprocal space. Integrated diffraction intensities were collected by a $\theta - 2\theta$ scan technique with scan rates varying from 1.5 to 14.65°/min (in 2θ) and a scan range of ±0.5° so that weaker reflections were examined more slowly to minimize counting errors. The data collected included $-1 \le h \le 11$, $-15 \le k \le 15$, $-14 \le l \le 14$, and $5.34° \le 2\theta \le 50.2°$ ($-1 \le h \le 9$, $-1 \le k \le 17$, $-22 \le l \le 22$, and $4.14° \le 2\theta \le 60.2°$) [$-1 \le h \le 10$, $-7 \le k \le 22$, $-7 \le l \le 7$, and $4.52° \le 2\theta \le 45.0°$]. During data collection, the intensities of three standard reflections were monitored every 97 reflections to check for crystal stability and alignment; no decay was observed during data collection. In total, 3568 (5558) [1251] reflections were collected, with 2442 (4042) [538] unique reflections remaining after averaging of equivalent reflections. An empirical absorption correction was applied to the data with a ψ-scan method. Corrections were made for Lorentz and polarization effects.

Solution and Refinement of the Structures. The XPREP program[66] was used to confirm the unit cell dimensions and the crystal lattice. Solutions were obtained with a Patterson function which located the heavy atoms. Successive difference Fourier syntheses revealed the positions of the light atoms, which were assigned on the basis of their bond distances to the heavy atoms. The final refinement was obtained by introducing anisotropic thermal parameters for all the atoms and a weight function and gave rise to a residual, R_1, of 0.0649 ($wR_2 = 0.1112$) (0.0533 ($wR_2 = 0.1158$)) [0.0402 ($wR_2 = 0.0822$)]. All calculations were performed on a Silicon Graphics 4600PC workstation using the SHELXL software package for structure solution and refinement and for molecular graphics.[66]

Nuclear Magnetic Resonance Spectroscopy. Nuclear magnetic resonance spectra were recorded unlocked (field drift <0.1 Hz h^{-1}) on a Bruker AC-300 (7.0463 T) spectrometer equipped with an Aspect 3000 computer. The ^{1}H, ^{13}C, and ^{19}F spectra were acquired with a 5-mm ^{1}H/^{13}C/^{31}P/^{19}F combination probe. The ^{99}Tc spectra were obtained with a 10-mm broad-band VSP probe (tunable over the range 23−202 MHz). The ^{19}F (282.409 MHz) spectra were recorded using a ∼90° pulse width of 7 μs. A total of 2000 transients were acquired in 32K memories using spectral width settings of 50 kHz, acquisition times of 0.328 s, resolutions of 3.05 Hz/data point, and line broadenings of 1 Hz. The ^{99}Tc (67.555 MHz) spectra were recorded using a ∼90° pulse width of 9 μs. A total of 2000 transients were acquired in 16K memories using spectral width settings of 50 kHz, acquisition times of 0.164 s, resolutions of 6.10 Hz/data point, and line broadenings of 10 Hz. The ^{1}H (300.133 MHz) spectra were recorded using a ∼90° pulse width of 2 μs. A total of 200 transients were acquired in 16K memories using spectral width settings of 3.6 kHz, acquisition times of 2.277 s, resolutions of 0.44 Hz/data point, and line broadenings of 0.3 Hz. The ^{13}C (75.469 MHz) spectra were recorded using a ∼90° pulse width of 2 μs. A total of 10 000 transients were acquired in 16K memories using spectral width settings of 18 kHz, acquisition times of 0.459 s, resolutions of 2.18 Hz/data point, and line broadenings of 2 Hz. Spectra have been referencing with respect to neat $CFCl_3$ (^{19}F), neat TMS (^{1}H, ^{13}C), and aqueous TcO_4^- (^{99}Tc) at 30 °C.

Raman Spectroscopy. Raman spectra were recorded as previously described[67] using 514.5-nm excitation. The spectra of thermally stable samples were recorded at room temperature on the spinning samples (ca. 5 Hz) which were sealed inside Pyrex melting point capillaries dried at 250 °C under vacuum. The spectra of thermally unstable samples were recorded at −150 °C in 4-mm FEP tubes using the macrochamber of the instrument. Low temperatures were achieved as previously described.[67] The Raman spectrometer was frequency-calibrated using the 1018.3-cm^{-1} line of neat indene. The laser power was approximately 300 mW at the sample (900 mW output power), and the monochromator slits were set to 200 μm, corresponding to a resolution of 1 cm^{-1}. A total of 10 reads having 30−60 s integration times were summed for the Raman spectra. Depolarization measurements were obtained using the macrochamber of the instrument and method VII described by Claassen et al.[68]

Calculations. All calculations were done at the density functional theory level with the program DGauss[69−71] (DGauss is a density functional program which is part of Unichem and is available from Oxford Molecular) on SGI computers. The DZVP basis set[72] and the A1 fitting set were used for H, O, F, and Tc in the all-electron calculations. For the effective core potential (ECP) and pseudopotential (PP) calculations, the DZVP2 basis set[72] for H, O, and F was used with the A1 fitting set. For the ECP and the PP calculations, the core electrons for Tc and Re were replaced with a PP or an ECP and the remaining electrons were treated with a polarized double-ζ basis set. We used PP's[32,33] that included only valence electrons so that there were 36 electrons in the core for Tc and 54 electrons in the core for Re. For the ECPs, we used the ECPS of Ermler et al.[29,30] and of Hay and Wadt.[26−28] The small-core versions of these were used so that there

(66) Sheldrick, G. M. *SHELXL*, Release 5.03; Siemens Analytical X-ray Instruments Inc.: Madison, WI, 1994.

(67) Casteel, W., Jr.; Kolb, P.; LeBlond, N.; Mercier, H. P. A.; Schrobilgen, G. J. *Inorg. Chem.* **1996**, *35*, 929.

(68) Claassen, H. H.; Selig, H.; Shamir, J. *Appl. Spectrosc.* **1969**, *23*, 8.

(69) Andzelm, J.; Wimmer, E.; Salahub, D. R. In *The Challenge of d and f Electrons: Theory and Computation*; Salahub, D. R., Zerner, M. C., Eds.; ACS Symposium Series, No. 394; American Chemical Society: Washington, DC, 1989; p 228.

(70) Andzelm, J. In *Density Functional Theory in Chemistry*; Labanowski, J., Andzelm, J., Eds.; Springer-Verlag: New York, 1991; p 155.

(71) Andzelm, J. W.; Wimmer, E. *J. Chem. Phys.* **1992**, *96*, 1280.

(72) Godbout, N.; Salahub, D. R.; Andzelm, J.; Wimmer, E. *Can. J. Chem.* **1992**, *70*, 560.

were 28 electrons in the core for Tc and 46 electrons in the core for Re. On the basis of our previous work on these types of metal compounds,[11,12] we performed the calculations at the local level with Slater exchange[73] and the correlation potential fit of Vosko, Wilk, and Nusair.[74] The geometries were optimized by using analytical gradient methods, and second derivatives were also calculated analytically.

Acknowledgment. We thank the donors of the Petroleum Research Fund, administered by the American Chemical Society, for support of this work under Grant ACS-PRF 31198-AC3. This research was performed in part using the Molecular Science Computing Facility (MSCF) in the William R. Wiley Environmental Molecular Sciences Laboratory at Pacific Northwest National Laboratory. MSCF is funded by the Office of Biological and Environmental Research, U.S. Department of Energy. Pacific Northwest is operated by Battelle for the U.S. Department of Energy under Contract DE-AC06-76RLO 1830. We thank the Natural Sciences and Engineering Research Council of Canada for the award of graduate scholarships to N.L. and the Canada Council for the award of a Killam Research Fellowship (1998−1999) to G.J.S. We also thank Dr. Hélène P. A. Mercier for her helpful comments and assistance in preparing the original manuscript.

(73) Slater, J. C. *Adv. Quantum Chem*. **1972**, *6*, 1.
(74) Vosko, S. J.; Wilk, L.; Nusair, W. *Can. J. Phys*. **1980**, *58*, 1200.

Supporting Information Available: Unit cell diagrams and X-ray crystallographic files in CIF format, for $TcO_2F_3 \cdot SbF_5$, $ReO_2F_3 \cdot SbF_5$ and $TcO_2F_3 \cdot XeO_2F_2$. This material is available free of charge via the Internet at http://pubs.acs.org.

IC9908221